2012

Surface state engineering of molecule–molecule interactions

Geoffrey Rojas
University of Nebraska-Lincoln, geoff.rojas@gmail.com

Scott Simpson
State University of New York at Buffalo, ssimpson@sbu.edu

Xumin Chen
University of Nebraska-Lincoln, xuminche@unlserve.unl.edu

Donna A. Kunkel
University of Nebraska-Lincoln, donna.ann.kunkel@gmail.com

Justin Nitz
University of Nebraska-Lincoln, jnitz3@hotmail.com

See next page for additional authors

Published in *Physical Chemistry Chemical Physics* 14 (2012), pp. 4971-4976; doi: 10.1039/c2cp40254h

Submitted January 25, 2012; accepted February 20, 2012; published online February 20, 2012.

Surface state engineering of molecule–molecule interactions

Geoffrey Rojas,[1] Scott Simpson,[2] Xumin Chen,[1] Donna A. Kunkel,[1] Justin Nitz,[1] Jie Xiao,[1] Peter A. Dowben,[1] Eva Zurek,[2] and Axel Enders [1]

1. Department of Physics and Astronomy, University of Nebraska-Lincoln, Lincoln, NE 68588, USA
2. Department of Chemistry, State University of New York at Buffalo, Buffalo, NY 14260-3000, USA

Corresponding author — A. Enders, email axel@unl.edu

Abstract
Engineering the electronic structure of organics through interface manipulation, particularly the interface dipole and the barriers to charge carrier injection, is of essential importance to improve organic devices. This requires the meticulous fabrication of desired organic structures by precisely controlling the interactions between molecules. The well-known principles of organic coordination chemistry cannot be applied without proper consideration of extra molecular hybridization, charge transfer and dipole formation at the interfaces. Here we identify the interplay between energy level alignment, charge transfer, surface dipole and charge pillow effect and show how these effects collectively determine the net force between adsorbed porphyrin 2H-TPP on Cu(111). We show that the forces between supported porphyrins can be altered by controlling the amount of charge transferred across the interface accurately through the relative alignment of molecular electronic levels with respect to the Shockley surface state of the metal substrate, and hence govern the self-assembly of the molecules.

1. Introduction

The electronic properties of organics in contact with metal substrates depend on the alignment of the electronic levels and bands at the metal–organic interface and the resulting hybridization of states, as well as charge transfer to or from the adsorbate, the molecular band offsets,[1–3] the emergence of interaction-induced states,[4,5] the distortion of the molecules[6] as well as changes that may occur at the substrate surface.[7] Also key to the interface electronic structure is the presence of substrate surface states.[8] Generally, the properties of metal–organic interfaces are determined by a delicate balance of competing factors and experiments usually assess only the cumulative effect of many different contributions to the interface electronic structure.[6,7] The net charge transferred across the interface, the formation of charge dipoles, and the work function are intrinsically related effects. Often what is highlighted is the interface dipole or the work function, but the substrate surface states, a fundamental ingredient to the interface electronic structure, are often poorly described. Here we demonstrate the importance of the Shockley surface states[9] in establishing the interface electronic structure using the example of tetraphenyl porphyrins (2H-TPP) chemisorbed on Cu(111). The surface state interactions with the adsorbed molecular layers are important for the charge transfer between the substrate and the molecule and the resulting surface dipoles that ultimately strongly influence the intermolecular lateral interactions. The surface state can be shifted in energy by using Ag buffer layers of varied thickness on Cu(111), thereby determining the overlap of molecular levels with substrate surface metal bands,[2] the amount of charge transferred, and consequently the intermolecular forces. We can relate our findings to the observed strong repulsive intermolecular Coulomb forces and the repression of molecular self-assembly. We show that the molecule–molecule interactions can be changed from repulsive to attractive, a concept similar to the steering of the molecular growth *via* dipolar interaction.[37,38] What is new here is that this is achieved without chemical modification of the molecules, but rather by controlling the amount of charge transferred across the interface through surface state engineering using Ag buffer layers on the Cu(111).

2. Results and discussion

The 2D character of an adsorbed monolayer of 2H-TPP has been exploited for a comparative study of the occupied and unoccupied band structure of large ensembles with direct and inverse photoelectron spectroscopy (UPS and IPES), as well as of selected individuals with the tip of a scanning tunneling microscope (STM) in the local spectroscopy mode (STS). By this combination of local and area-integrating complementary methods the atomistic basis of observed features in the electronic structure became evident. STM images, taken at sub-monolayer to monolayer coverage of 2H-TPP on Cu(111), are shown in Figure 1. A coverage of θ = 1 ML is defined here as the maximum observed packing density within the first layer of 0.42 molecules per nm^2. This

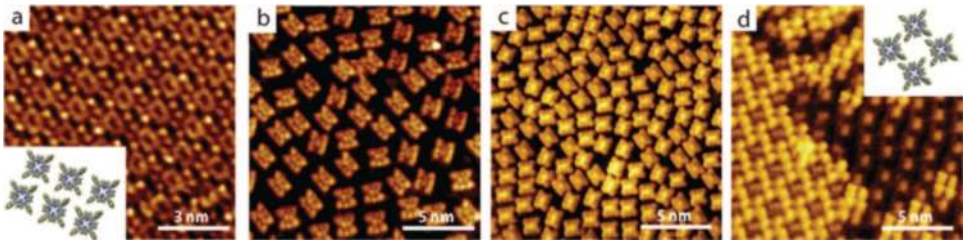

Figure 1. STM images of 2H-TPP on Ag(111) (a) and Cu(111) (b–d). The molecule coverage is 0.6 ML (b), 0.7 ML (c) and 1.2 ML (d). I_t = 0.4 nA, U_b = +0.8 V.

packing is 20% smaller, expressed in terms of areal density, than that observed on Ag(111), see Figure 1a.[10,11] The mobility of the molecules is sufficiently high for surface diffusion, as concluded from visible substrate step edge decoration (not shown), however, no island nucleation is observed. The molecules remain isolated and roughly equally spaced on the terraces of the Cu(111) (Figure 1b & c). They appear to be aligned along the three ⟨110⟩ crystallographic directions of the surface, concluded from the observed angles of multiples of 120° between the major axes of any two molecules.[38] It can be seen by comparing Figure 1b and c that molecules are added to the first monolayer even if the gaps between the molecules are significantly smaller than the size of the molecules itself. This requires rearrangement of all molecules in the layer during deposition. Self-organization of the 2H-TPPs into networks, as found for the same molecules on Ag(111) in Figure 1a and Au(111),[10–12] was not observed on Cu(111) at any coverage and sample temperature in the range between 77 K and 500 K. We do observe by inspection of Figure 1c and d, however, a behavior like in the case of a two-dimensional gas where the average intermolecular distance decreases with increasing coverage.[40] Also, an alignment of the molecules relative to each other sets in as the areal density of the molecules increases. Upon reaching saturation coverage within the first layer, molecules nucleate into islands on top of the first layer. The architecture of this arrangement is a porous 2D network apparently dominated by π–π bonds, and is a different architecture than the densely packed arrangement observed for the same molecules on Ag(111) in Figure 1a. We conclude from these observations that the net force between the molecules within the first layer is repulsive, while it is attractive for the molecules within the second layer.

The occupied and unoccupied electronic structure of the adsorbate–substrate system has been studied in detail with tunneling spectroscopy and combined photoemission and inverse photoemission spectroscopies, as seen in Figure 2. The combined photoemission spectra of the 2H-TPP covered Cu(111) show characteristic peaks that are not observable in the spectra of the pristine Cu(111). One feature, at +2 eV, is in reasonable agreement with the lowest unoccupied molecular orbital (LUMO) of calculated and measured spectra for similar TPP systems.[13] Also the spectra of the occupied states resemble those reported for 2H-TPP adsorbed on other noble-metal systems,[14] with the highest occupied molecular orbital (HOMO) at approximately −2 eV. Within this HOMO–LUMO gap we observe an additional characteristic peak at +0.65 eV at sub-monolayer coverage, which is observed to decay rapidly in intensity with increasing coverage and is not apparent in the spectra at 3 ML coverage or more.

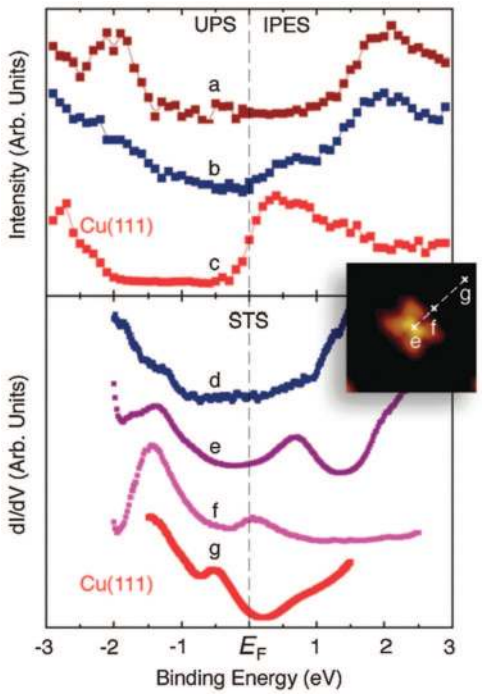

Figure 2. *Upper panel:* Photoemission (UPS) and inverse photoemission (IPES) spectra of 2H-TPP on Cu(111). (a) 3 ML 2H-TPP; (b) 1 ML 2H-TPP; (c) bare Cu(111). *Lower panel:* STS point spectra taken on or near lone TPP molecules. (d) On top of a molecule in the second layer; (e) on top of a molecule in the first layer; (f) on Cu, at a distance of 1 Angstrom from the molecule edge; (g) on Cu, several Angstroms away from a molecule. Inset: STM image showing the positions where spectra (e–g) were taken. Binding energies are denoted as E–E_F making occupied state energies negative and unoccupied states positive.

Complementary to the combined photoemission and inverse photoemission spectroscopy measurements, point spectroscopy measurements have been taken locally with STS over a similar energy range, see bottom panel in Figure 2. Single point dI/dV spectra were taken over the molecules themselves, as well as the surrounding Cu surface at successively increasing distance from the molecule center. The observed HOMO and LUMO of the molecules are aligned well with those observed using photoelectron spectroscopy; the LUMO is seen at approx. 1.5 eV above the Fermi level, contained with the LUMO+1 peak. The spectra taken on the bare Cu show the well-known Shockley surface state at −0.4 eV,[15,16] which is not resolved in the photoelectron spectra. This surface state is suppressed on the Cu surface covered with $\theta \geq 0.7$ ML 2H-TPP. At lower coverage, this surface state is shifted towards the Fermi level in the direct vicinity of the

molecule. The spectra shown in Figure 2f were taken at a distance of 6 Å from the molecule center and show this surface state shifted upward in energy by $\Delta E \approx 0.4$ eV. Also within the HOMO–LUMO gap at +0.65 eV an electronic state, already known from the IPES measurements, is observed at the molecules. This peak is only observed for spectra taken of molecules in the first monolayer. Spectra taken of molecules in the second layer do not show this substrate surface state feature, and yet the characteristic LUMO and HOMO remain undisturbed.

The molecules of the second layer appear in the STM images under the same tunneling conditions with dark center and bright phenyl arms, while in the first layer the opposite is observed, the centers are bright and the phenyl arms are dark. This change in contrast is due to an electronic level rearrangement at the interface.[5] We again exploit the local nature of tunnel spectroscopy to identify local differences in the DOS. In STS point spectra taken at the center of a molecule in the second layer the new peak at +0.65 eV, observed over the molecules in the first layer, does not appear. This allows us to attribute the physical origin of this state to the 2H-TPP/Cu interface. The electronic states in this energy range have been observed previously for other porphyrin-based surface systems on Ag(111) as well as Cu(111) with photoelectron spectroscopy,[5,17,18] and have been heretofore ascribed to the shifted LUMO of the porphyrin macrocycle. However, the absence of the energy state at +0.65 eV in the second monolayer provides now evidence that this state is an interface state.

Measurements of the local work function, Φ, have also been made using the STM. We have characterized and measured the local work function to evaluate the local surface dipoles, following a procedure similar to that published in Reference 19 and described in the Supplementary Information. The so measured work function of the Cu(111) is $\Phi_{Cu} = (4.9 \pm 0.2)$ eV. With 2H-TPP deposited, we find a decrease of the work function by $\Delta\Phi \approx (-2.0 \pm 0.5)$ eV over the center of TPP molecules, and an increase of $\Delta\Phi \approx +(1.0 \pm 0.4)$ eV at the boundary of the molecule's macrocycle. While these data are in quantitative agreement with the net work function shift of 0.84 eV found for 1 ML 2H-TPP on Ag(111),[5] the particular advantage of these local measurements is that they reveal a significant amount of spatial variance. For clarification of the spatial variance, a map of the work function has been measured in a square area across the molecule and its surrounding from 100 × 100 separately performed point spectra. This Φ-map is shown together with an STM image of a lone 2H-TPP on Cu(111) in Figure 3. By comparing both results in this manner the spatial dependence of the work function can be associated with local chemical components of the adsorbed molecule, and with the locally measured density of states. The Φ drops significantly over the location of the central pyrolines while increasing relatively to the bare Cu(111) over the surrounding hydrogen edges and phenyl ligands. Surrounding the molecule in a narrow band there is a slight drop in the Cu(111) work function. This band corresponds to the area where the upward shift in the surface state was observed, too.

The electronic interactions at the 2H-TPP/Cu and the 2H-TPP/Ag interfaces can be understood using the results of dispersion corrected density functional theory (DFT-D) calculations, undertaken as described in the Supplementary Information. The computational results, summarized in Table 1, show that the binding energy of the molecules to the substrate is significantly larger on Cu(111) (5.31 eV) than on Ag(111) (3.1 eV), resulting in a shorter distance between the molecule and the substrate and increased distortion of the molecule on Cu(111) (Figure 4). The latter number is in good agreement with the 2.8 eV computed using the mixed Gaussian plane wave scheme.[45] In particular, the dihedral angle of the phenyl ligands changes and the ligands become nearly planar to the surface. For comparison, we calculate the free 2H-TPP molecule as having a dihedral angle of 62.7°, in agreement with ref. 10, 20–22 and 45. This distortion is visible in the STM images in Figure 1b, and in agreement with recently reported results.[39,41] As a result of the rotation of the phenyl arms, the pyrrole rings containing the N–H motifs distort downwards so that the shortest distance between one of their carbons and the surface is 2.62/2.86 Å for Cu/Ag. The pyrrole rings containing the lone or iminic nitrogen atoms distort upwards and the largest distance between one of their carbons and the surface is 4.10/4.25 Å for Cu/Ag. The dispersion interaction was calculated to be greater between 2H-TPP and Cu(111) than with Ag(111) (9.2 *vs.* 5.7 eV), and—as shown in the Supplementary Information—so were other contributions to the binding energy.

The composition of the molecular orbitals of the metal–adsorbate system was decomposed into contributions from occupied and unoccupied orbitals of the finite copper cluster and of the 2H-TPP. The resulting interaction diagram showed that the binding in this system can largely be explained by the Dewar, Chatt and Duncanson model which has, for example, been applied to benzene on Cu(110).[46] The charge redistribution upon adsorption is in part due to electron donation from the HOMO of 2H-TPP to the metal surface, and back donation from the surface to the LUMO. Because of the decreased metal–adsorbate distance (increased overlap), the molecule/surface states are more disperse for

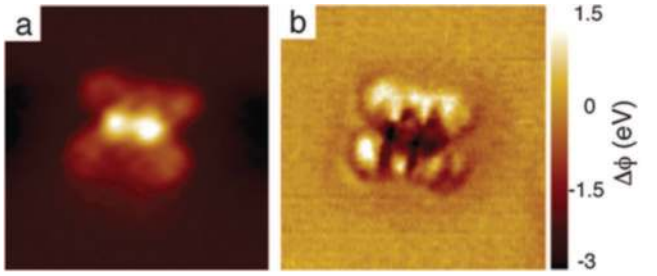

Figure 3. (a) STM image of a lone 2H-TPP molecule on Cu(111). I_T = 0.4 nA, U_b = +0.8 V; image size 4 nm × 4 nm. (b) Work function map of the same molecule, showing lowered work function at the center of the molecule and increased work function at the boundary of the molecule, relative to the substrate.

Table 1 The binding energy (E_b), charge and structure of 2H-TPP on top of Cu(111) and Ag(111). The surface distances, d_{Cu} and d_{Ag}, are the average calculated distances of the central nitrogen atoms of the 2H-TPP to the metal. The dihedral angle is the angle with respect to the macrocycle, and is defined in the Supplementary Information.

System	E_b/eV	Surface charge	Dihedral angle/°	Surface distance, d/Å
Cu(111)	5.31	−0.89	38.3	3.05
Ag(111)	3.07	−0.46	42.1	3.30

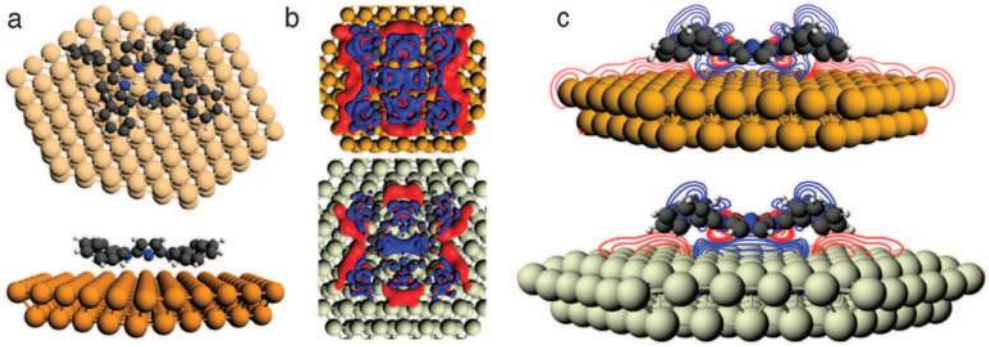

Figure 4. (a) Top and side view of the optimized geometry of 2H-TPP on top of a Cu(111) slab. (b) Top views and (c) side views of the calculated differences between the charge density of the metal–organic systems and that of the isolated, distorted fragments. They illustrate how the charge density changes upon adsorption of the 2H-TPP molecule to the metal surfaces Cu(111) (top) and Ag(111) (bottom), with blue being a decrease and red an increase. The same isovalue of ±0.0003 au was employed to obtain all contours. The lone N-pair is aligned horizontally in (b).

the Cu(111) surface. Our findings are in agreement with the increase in nobleness of a metal descending down Group 11 from Cu to Ag to Au.[2] The build up of charge surrounding the copper–molecule interface (the red isovalue in Figure 4c), along with the charge on the molecules themselves, both which are much larger for the 2H-TPP–Cu system than for 2H-TPP–Ag, prevents the adsorbate molecules from interacting with one another due to electrostatic repulsion, thereby impeding self-assembly on the Cu(111) surface.

The charge density difference plots in Figure 4 reflect strong variations in the charge density at the interface upon adsorption: there is charge depletion (blue) directly under the center of the molecules and an increase in the charge density (red) along the edges of the molecule and under the phenyl ligands. The underlying mechanism here is Pauli repulsion, which follows from the quantum mechanical requirement that overlapping electronic states must be orthogonal to each other. This drives up the energy and as a result pushes charge away at the surface of the Cu in an area directly under the center of the molecule. This effect has been described as the "pillow effect."[3,23–25] The redistribution and exchange of charge also changes drastically the surface dipole of the Cu and is at the origin of the observed spatial variation of the work function. By comparison, the smaller charge transfer from Ag to the adsorbate is in line with a weaker binding energy, a longer metal–adsorbate distance and a smaller pillow effect occurring on the metal's surface.

Besides the electrostatic repulsion between the molecules there are also attractive interactions, mainly van-der-Waals and dispersive interactions. Additional bonding contributions come from CH–π and π–π interactions between the phenyl ligands. For a freestanding 2H-TPP dimer, the total binding energy was estimated to be 0.3 eV. The net effect is thus dependent on the competition between Coulomb repulsion and the mainly van der Waals attraction. The net force is attractive for 2H-TPP on Ag(111) and Au(111)[10,18,26] and repulsive on Cu(111), owing to the discussed differences in charge transferred and Coulomb repulsion. A similar dominance of the electrostatic repulsion has been reported earlier for other organic–metallic interface systems.[10,27–30,38] In addition here, the distorted phenyl arms of the molecules impede the formation of π–π bonds, thereby further decreasing the propensity of binding between two 2H-TPP molecules.

Our experimental and computational results are suggesting strong interaction between the TPP and the Cu(111) surface. Very recent publications by Doyle *et al.*[41] and Buchner *et al.*[39] have in fact proposed that the two iminic nitrogens in the TPP form an intermediate complex with copper atoms in the surface layer, which aligns the molecules along the ⟨110⟩ directions of the substrate surface. This provides a good explanation for the alignment of the molecules in Figure 1b and c. Our presented DFT calculations reveal now additional details about the bond length, the role of the iminic nitrogens in the bonding of the molecule to the substrate, their charge and geometry.

The observed differences in the interactions of 2H-TPP on Ag and Cu surfaces were exploited to actually control the inter-molecular forces, between the repulsive and attractive limits by engineering the metal–organic interface. The trick is to deposit the molecules on the Cu(111), which was pre-covered by an Ag buffer layer of variable thickness. We refer to the literature for structural details of heteroepitaxial Ag on Cu(111).[42–44] The STM images of 2H-TPP adsorbed on 1 to 3 monolayers of Ag on Cu(111) are shown in Figure 5. Clearly, the molecules remain, more or less, statistically distributed on 1 ML Ag/Cu, while islands of extended networks, identical in architecture to that found on Ag(111) in Figure 1a, are observed for the 2H-TPP adsorbed on 3 ML Ag/Cu. At the intermediate Ag buffer layer thickness of 2 ML, clusters of 2H-TPP adsorbed molecules are commonly observed but with noticeable degree of disorder within such clusters. On Ag layers on Cu, the 2H-TPP molecules appear in 2 distinctively different symmetries: the symmetry labeled (i) which is usually observed on Cu(111), and the symmetry labeled (ii) which is typical for TPP on Ag(111). With increasing Ag layer thickness, the occurrence of 2H-TPP molecules in configurations of type (i) decreases while at the same time the occurrence of the 2H-TPP adsorbed molecules in the arrangement of type (ii) increases. It appears as if clusters of molecules, ordered or disordered, are mostly formed by 2H-TPP adsorbed molecules of type (ii). We ascribe this difference in the conformation to differences in the molecule–substrate complex formation proposed in ref. 41. This implies that there is some degree of intermixing with the Cu substrate in the first Ag layer.

Tunneling spectroscopy was again employed to elucidate the local electronic structure of the interface. A work function

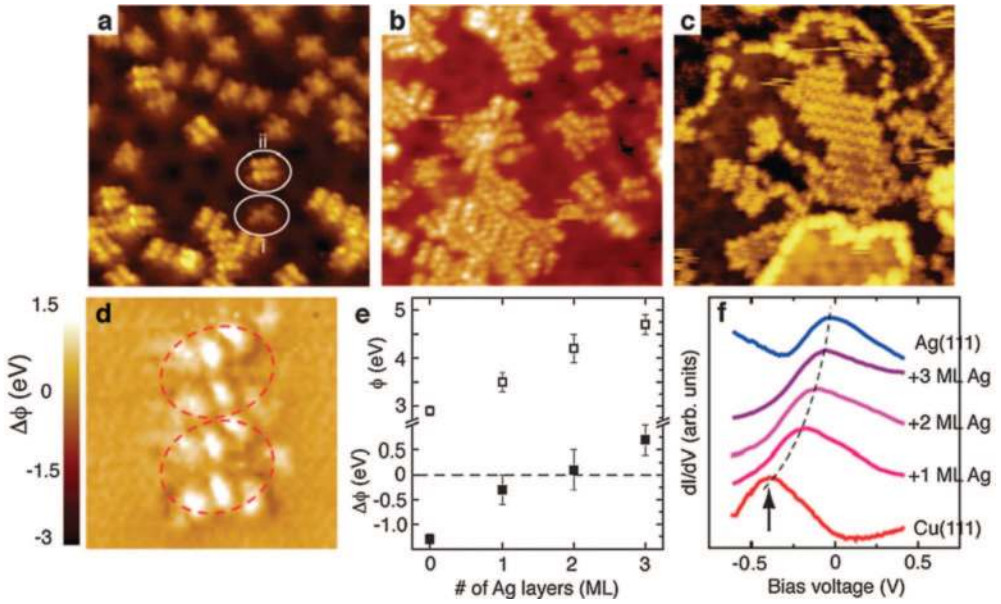

Figure 5. STM images of 2H-TPP on Ag buffer layers of thickness t_{Ag} on Cu(111) where t_{Ag} = 1 ML (a), t_{Ag} = 2 ML (b), t_{Ag} = 3 ML (c). Two different shapes of the molecules are observed, labeled (i) and (ii), see text for explanation. Image size 15 nm × 15 nm. (d) Work function map of a TPP dimer on 2 ML Ag/Cu(111). The position of each TPP is circled. The color bar is the same as in Figure 3. (e) Work function measured locally in the center of a TPP molecule, as a function of Ag thickness (open square), and the change in the work function compared to the substrate, $\Delta\varphi$, obtained from integrating over one TPP molecule (solid square). (f) STS point spectra on Cu, Ag films on Cu, and Ag substrates showing the Shockley surface state.

map of a TPP dimer on 2 ML Ag/Cu(111) is shown in Figure 5d, using the same color scale as in Figure 3b. Evidently, there is no significant decrease of the work function as compared to the bare Ag/Cu system in the center of the molecule, in sharp contrast to our observation for TPP on Cu(111). This is further reflected in the trend of the work function as a function of Ag spacer thickness, shown in Figure 5e. Both, the work function measured locally in the center of a TPP molecule as well as the work function averaged over one molecule, are plotted for comparison. Strikingly, there is a strong dependence of the work function near the center of the molecules on the thickness of the Ag layer, revealing that the Ag thickness governs the charge distribution at the metal–organic interface. The work function integrated over a molecule is changing its sign from an overall decrease compared to the substrate to an increase at t_{Ag} = 2 ML, which is the coverage where also TPP cluster formation sets in. The local spectrum of electronic states taken on top of the molecules is similar for all samples in Figure 5a–c (not shown). However, the Shockley surface state of the substrate on the other hand shifts upward in energy with increasing thickness of the Ag buffer layer, from −400 meV for clean Cu(111) to −50 meV for Ag(111) (Figure 5f). The energy of this Shockley state is thus a precise indicator for the Ag layer thickness. Key is that the energy of the Shockley state can be adjusted by the Ag buffer layer thickness between the two extremes of pure Ag(111) and Cu(111) surfaces.

3. Conclusions

It has been already established that the electronic level alignment at the metal–organic interface and frontier orbital symmetry determines the hybridization of levels and the amount of charge transferred across the interfaces.[1,31] Based on the results shown here, we find it reasonable to assume that the Shockley state plays a crucial role for the interaction strength. Depending on the exact energetic position of this state, more or less overlap with the corresponding molecule levels is possible, thereby facilitating (Cu) or impeding (Ag) charge transfer across the interface. By controlling the exact energetic position of the surface state by the choice of thickness of Ag buffer layers on Cu(111), the degree of electronic level hybridization can thus be finely tuned, to adjust the amount of charge transferred and the strength of the Coulomb repulsion. Since the van der Waals interaction remains unaffected by this, the net effect can thus be chosen to be repulsive or attractive. The ability to control inter-molecular forces for a particular type of molecule between both extremes in this manner opens new possibilities to steer molecular self-assembly, especially if patterned buffer layers are used. It is thus an important new milestone in establishing rational design principles for organics in contact with surfaces. Specifically, we demonstrated the potential of using substrates to build organic structures and frameworks of potentially greater complexity than currently possible, exhibiting pre-defined and desired functionality.

4. Experimental

The experiments were carried out using an Omicron low temperature scanning tunneling microscope in an ultrahigh vacuum system with a base pressure of 8×10^{-11} mbar. Single crystalline substrates have been cleaned in UHV by Ar^+ ion sputtering and annealing. TPP molecules have been deposited by thermal evaporation from a home-built Knudsen cell, with the substrate held at room temperature. The combined photoemission and inverse photoemission spectroscopy measurements have been performed in a second UHV system[32] but using the same substrates and Knudsen cells.

The DFT-D calculations were carried out using the ADF software package.[33,34] The revPBE gradient density functional[35] was employed, and Grimme's latest dispersion corrected functional[36] was used to account for the dispersion forces. Tests were performed to determine the effect of the basis set on the binding energy of benzene to an Ag(111) slab. For the results given in the main text, the basis functions on all of the atoms consisted of a valence triple-ζ Slater-type basis set with polarization functions (TZP) from the ADF basis-set library. The core shells up to 1s, 1s, 3p and 4p of carbon, nitrogen, copper and silver, respectively, were kept frozen. A Hirschfeld charge analysis was used to determine the magnitude of the charge transferred between the adsorbate and the metal surface. More computational details and complementary results are provided in the Supplementary Information.

Acknowledgments — This work was supported by the National Science Foundation, in parts by the NSF grants DMR-0747704 (CAREER), DMR-0213808 (MRSEC) and CHE-0909580 grant EPS-1004094. Support from the Center of Computational Research at SUNY Buffalo is acknowledged.

References

1 H. Ishii, K. Sugiyama, E. Ito and K. Seki, *Adv. Mater.*, 1999, **11**(8), 605–625
2 B. Hammer and J. K. Nørskov, *Nature*, 1995, **376**, 238
3 P. S. Bagus, K. Hermann and Ch. Wöll, *J. Chem. Phys.*, 2005, **123**, 184109
4 R. Temirov, S. Soubatch, A. Luican and F. Tautz, *Nature*, 2006, **444**, 350–353
5 T. Lukasczyk, K. Flechtner, L. R. Merte, N. Jux, F. Maier, J. M. Gottfried and H.-P. Steinrück, *J. Phys. Chem. C*, 2007, **111**, 3090–3098
6 L. Romaner, G. Heimel, J.-L. Brédas, A. Gerlach and F. Schreiber, *Phys. Rev. Lett.*, 2007, **99**, 256801
7 S. Bedwani, D. Wegner, M. F. Crommie and A. Rochefort, *Phys. Rev. Lett.*, 2008, **101**, 216105
8 A. Scheybal, K. Müller, R. Bertschinger, M. Wahl, A. Bendounan, P. Aebi and T. A. Jung, *Phys. Rev. B: Condens. Matter*, 2009, **79**, 115406
9 W. Shockley, *Phys. Rev.*, 1939, **56**, 317
10 G. Rojas, X. Chen, C. Bravo, J. Kim, J.-S. Kim, J. Xiao, P. A. Dowben, Y. Gao, X. C. Zeng, W. Choe and A. Enders, *J. Phys. Chem. C*, 2010, **114**, 9408–9415
11 J. Brede, M. Linares, S. Kuck, J. Schwöbel, A. Scarfato, S.-H. Chang, G. Hoffmann, R. Wiesendanger, R. Lensen, P. H. J. Kouwer, J. Hoogboom, A. E. Rowan, M. Bröring, M. Funk, S. Stafström, F. Zerbetto and R. Lazzaroni, *Nanotechnology*, 2009, **20**, 275602
12 F. Buchner, K. Flechtner, Y. Bai, E. Zillner, I. Kellner, H.-P. Steinrück, H. Marbach and J. M. Gottfried, *J. Phys. Chem. C*, 2008, **112**, 15458
13 R. Thorpe, R. A. Bartynski, J. Rochford, S. Rangan, S. Katalinic and E. Galoppini, *J. Phys. Chem. C*, 2010, **114**, 1139–1147
14 M.-S. Liao and S. Scheiner, *J. Chem. Phys.*, 2002, **117**(1), 205
15 S. D. Kevan, *Phys. Rev. Lett.*, 1983, **50**, 526
16 O. Jeandupeux, L. Bürgi, A. Hirstein, H. Brune and K. Kern, *Phys. Rev. B: Condens. Matter*, 1999, **59**(24), 15926–15934
17 W. Auwärter, K. Sufert, F. Klappenberger, J. Reichert, A. Weber-Bargioni, A. Verdini, D. Cvetko, M. Dell' Angela, L. Floreano, A. Cossaro, G. Bavdek, A. Morgante, A. P. Seitsonen and J. V. Barth, *Phys. Rev. B: Condens. Matter*, 2010, **81**(24), 245403
18 K. Comanici, F. Buchner, K. Flechtner, T. Lukasczyk, M. Gottfried, H.-P. Steinrück and H. Marbach, *Langmuir*, 2008, **24**(5), 1897–1901
19 L. Vitali, G. Levita, R. Ohmann, A. Comisso, A. De Vita and K. Kern, *Nat. Mater.*, 2010, **9**, 320–323
20 W. Auwärter, A. Weber-Bargioni, A. Riemann, A. Schiffrin, O. Gröning, R. Fasel and R. J. V. Barth, *J. Chem. Phys.*, 2006, **124**(19), 194708
21 W. Auwärter, A. Weber-Bargioni, S. Brink, A. Riemann, A. Schiffrin, M. Ruben and J. V. Barth, *ChemPhysChem*, 2007, **8**, 250
22 F. Buchner, K.-G. Warnick, T. Wölfle, A. Görling, H.-P. Steinrück, W. Hieringer and H. Marbach, *J. Phys. Chem. C*, 2009, **113**, 16450–16457
23 P. S. Bagus, V. Staemmler and Ch. Wöll, *Phys. Rev. Lett.*, 2002, **89**, 096104
24 H. Vázquez, Y. J. Dappe, J. Ortega and F. Flores, *Appl. Surf. Sci.*, 2007, **254**, 378
25 P. C. Rusu, G. Giovannetti, C. h. Weijtens, R. Coehoorn and G. Brocks, *Phys. Rev. B: Condens. Matter*, 2010, **81**, 125403
26 Z. C. Dong, X. L. Zhang, H. Y. Gao, Y. Luo, C. Zhang, L. G. Chen, R. Zhang, X. Tao, Y. Zhang, J. L. Yang and J. G. Hou, *Nat. Photonics*, 2010, **4**, 50–54
27 D. Wegner, R. Yamachika, Y. Wang, V. W. Brar, B. M. Bartlett, J. R. Long and M. F. Crommie, *Nano Lett.*, 2008, **8**(1), 131–135
28 I. Fernandez-Torrende, S. Monturet, K. Franke, J. Fraxedas, N. Lorente and J. Pascual, *Phys. Rev. Lett.*, 2007, **99**, 176103
29 Z. G. Soos and B. J. Topham, *Org. Electron.*, 2011, **12**, 39–44
30 C. Wagner, D. Kasemann, C. Golnik, R. Forker, M. Esslinger, K. Müllen and T. Fritz, *Phys. Rev. B: Condens. Matter*, 2010, **81**, 035423
31 H. Vázquez, R. Oszwaldowski, P. Pou, J. Ortega, R. Pérez, F. Flores and A. Kahn, *Europhys. Lett.*, 2004, **65**, 802
32 J. Zhang, D. N. McIlroy, P. A. Dowben, H. Zeng, G. Vidali, D. Heskett and M. Onellion, *J. Phys.: Condens. Matter*, 1995, **7**, 7185
33 G. te Velde, F. M. Bickelhaupt, E. J. Baerends, C. Fonseca Guerra, S. J. A. van Gisbergen, J. G. Snijders and T. Ziegler, *J. Comput. Chem.*, 2001, **22**, 931–967
34 E. J. Baerends, J. Autschbach, A. Bérces, F. M. Bickelhaupt, C. Bo, P. M. Boerrigter, L. Cavallo, D. P. Chong, L. Deng and R. M. Dickson, *et al.*, *ADF2006.01, SCM, Theoretical Chemistry*, Vrije Universiteit, Amsterdam, The Netherlands; http://www.scm.com
35 J. P. Perdew, K. Burke and Y. Wang, *Phys. Rev. B: Condens. Matter*, 1996, **54**, 16533–16539
36 S. Grimme, J. Antony, S. Ehrlich and H. Krieg, *J. Chem. Phys.*, 2010, **132**, 154104
37 S. Kuck, S.-H. Chang, J.-P. Klöckner, M. H. Prosenc, G. Hoffmann and R. Wiesendanger, *ChemPhysChem*, 2009, **10**, 2008–2011
38 Ch. Stadler, S. Hansen, I. Kröger, Ch. Kumpf and E. Umbach, *Nat. Phys.*, 2009, **5**, 153–158
39 (*a*) F. Buchner, J. Xiao, E. Zillner, M. Chen, M. Röckert, S. Ditze, M. Stark, H.-P. Steinrück, J. M. Gottfried and H. Marbach, *J. Phys. Chem. C*, 2011, **115**, 24172–24177 ; (*b*) F. Buchner, E. Zillner, M. Röckert, S. Glässel, H.-P. Steinrück and H. Marbach, *Chem.–Eur. J.*, 2011, **17**, 10226–10229
40 T. Yokoyama, T. Takahashi and K. Shinozaki, *Phys. Rev. Lett.*, 2007, **98**, 206102
41 C. M. Doyle, S. A. Krasnikov, N. N. Sergeeva, A. B. Preobrajenski, N. A. Vinogradov, Y. N. Sergeeva, M. O. Senge and A. A. Cafolla, *Chem. Commun.*, 2011, **47**, 12134–12136
42 E. Bauer, *Appl. Surf. Sci.*, 1982, **11–12**, 479
43 I. Meunier, G. Treglia, J.-M. Gay, B. Aufray and B. Legrand, *Phys. Rev. B: Condens. Matter*, 1999, **59**(16), 10910
44 K. Umezawa, S. Nakanishi, M. Yoshimura, K. Ojima, K. Ueda and W. M. Gibson, *Phys. Rev. B: Condens. Matter*, 2000, **63**, 035402
45 G. Di Santo, S. Blankenburg, C. Castellarin-Cudia, M. Fanetti, P. Borghetti, L. Sangaletti, L. Floreano, A. Verdini, E. Magnano, F. Bondino, C. A. Pignedoli, M. Nguyen, R. Gaspari, D. Passerone and A. Goldoni, *Chem.–Eur. J.*, 2011, **17**, 14354
46 L. Triguero, A. Föhlisch, P. Vaterlaein, J. Hasselström, M. Weinelt, L. G. M. Petterson, Y. Luo, H. Agren and A. Nilsson, *J. Am. Chem. Soc.*, 2000, **122**, 12310

Section 1: Computational Details

The DFT-D calculations were carried out using the ADF software package[1,2]. The revPBE gradient density functional[3-6] was employed, and Grimme's latest dispersion corrected functional[7] was used to account for the dispersion forces. Tests were performed to determine the effect of the basis set on the binding energy of benzene to an Ag(111) slab, see Section 3 below. For the results given in the main text, the basis functions on all of the atoms consisted of a valence triple-ζ Slater-type basis set with polarization functions (TZP) from the ADF basis-set library. The core shells up to 1s, 1s, 3p and 4p of carbon, nitrogen, copper and silver, respectively, were kept frozen. In situations where SCF convergence issues arose, the steepest decent method was employed. Both a Mulliken and a Hirshfeld charge analysis were used to determine the magnitude of the charge transferred between the adsorbate and the metal surface.

The Cu(111) and Ag(111) surfaces were simulated by using a finite slab, or cluster, comprised of 166 metal atoms and the experimental lattice parameter of 3.614 Å[8] and 4.086 Å[8], respectfully. The clusters were composed of two layers with the top layer containing 91 atoms and the bottom layer containing 75 atoms. During the structural relaxation, the top layer of the slabs was allowed to relax. Next, a geometry optimization was performed where the 2H-TPP was placed on-top of the optimized metal surface, and the coordinates of the cluster atoms were kept fixed. This procedure was found to give binding energies (BEs) in reasonable agreement with experimental data obtained for benzene adsorbed on Ag(111)/Cu(111) (see Section 3 of the Supplementary Information, SI). For select systems, the basis set superposition error (BSSE) was calculated using the Counterpoise method.

To clarify the nature of the bonding, a fragment orbital analysis was employed using the ADF program[1]. The fragments used were those of the metal cluster and distorted adsorbate (as found in the optimized structures **S3**, **S5**, **S6** and **S7**). The composition of the molecular orbitals of the metal-adsorbate system was decomposed into terms of occupied and unoccupied orbitals of the finite metal cluster and of the adsorbate. From this analysis, charge density difference (CDD) contours and isosurfaces were plotted using the ADFview program. The CDD given below are the calculated differences between the charge density of the metal-organic systems and that of the isolated fragments. They illustrate how the charge density changes upon adsorption of the molecule to the metal surface.

Section 2: 2H-TPP Dimer Binding Energies

The coordinates for the adjacent 2H-TPP dimer (**S1**) and the sandwich 2H-TPP dimer (**S2**) can be found in Section 5 of the SI. The basis functions on all of the atoms consisted of a valence triple-ζ Slater-type basis set with polarization functions (TZP) from the ADF basis-set library. The core shells up to 1s of carbon and nitrogen were kept frozen. The binding energy (BE) of **S1** was calculated as being 0.03 eV. The binding energy of **S2** was found to be 1.12 eV.

Figure 1: Illustrations of the geometries of the (a) adjacent (**S1**), and (b) sandwich (**S2**) 2H-TPP dimer.

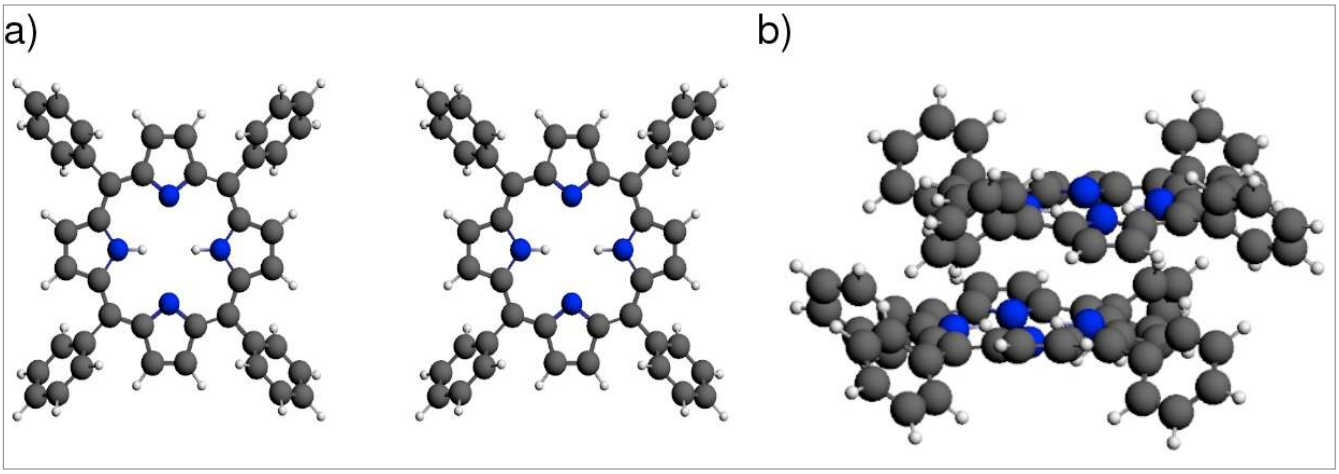

The most stable benzene dimer (**S8**)[9] has a geometry which is very similar to that of **S2**. Using the computational settings described herein, the binding energy for the benzene dimer was found to be 0.05 eV, which is somewhat smaller than that computed by high-level CCSD(T) calculations[9] for the parallel-displaced benzene dimer (0.09 to 0.12 eV).

Section 3: Benzene on Various Copper/Silver Surfaces

The geometries of benzene adsorbed to metal clusters (models for various metal surfaces) were optimized, and the BEs computed. In the following geometry optimizations the bottom layer of metal atoms was kept fixed, but the top layer of atoms was allowed to relax. For benzene adsorbed on the Ag(111) surface computations were performed using different basis sets, and varying the number of atoms in the cluster. The BE, given below in Table 1, were calculated by:

$$\mathrm{BE} = E_{(\text{Organic Molecule})} + E_{(\text{Metal Slab})} - E_{(\text{Organic-Metal Complex})} \quad (1)$$

Table 1: The binding energy (BE) of benzene to Ag(111) using various basis sets and slab sizes[a]

System	# of Surface Atoms	Adsorbate Basis	Surface Basis	BE (eV)
Benzene-Ag(111)	64	DZP	DZ	1.16
Benzene-Ag(111)	64	TZP	DZ	0.98
Benzene-Ag(111)	64	DZP	TZP	1.10
Benzene-Ag(111)	64	TZP	TZP	0.87
Benzene-Ag(111)	166	TZP	TZP	0.77
		Experimental BE[7]		0.56

[a] DZ denotes a double-ζ basis; DZP is a double-ζ basis with polarization functions; TZP is a triple-ζ basis set with polarization functions.

A TZP basis set on the adsorbate atoms and the surface atoms was found to give a BE which was closest to the experimental values. Moreover, as the number of atoms used to simulate the metallic slab increased, the computed BE was found to approach the experimental BE.

The computed BE between benzene and various copper/silver surfaces are given below in Table 2. The results shown in Table 1 and 2 illustrate that computational method employed overestimates the BE for these types of systems, in-line with the original benchmark calculations[7]. The BSSE lowers the computed BEs slightly. For example, the BSSE-corrected BE of benzene on Cu(111) and Ag(111) with 64 atoms in the cluster was found to be 1.11 and 0.79 eV, respectfully.

The optimized coordinates of the Ag(111)-benzene system with 64 silver atoms (**S3**), the Ag(111)-benzene system with 166 silver atoms (**S4**), and the Cu(111)-benzene system (**S5**) can be found in Section 5 of the SI.

Table 2: The binding energy (BE) of benzene to various copper and silver surfaces[a]

System	Calculated BE (eV)	Experimental BE (eV)
Cu(100)-Benzene[b]	1.03	-
Cu(110)-Benzene[c]	1.27	0.73[10]
Cu(111)-Benzene[d]	1.28	0.59[11]
Ag(100)-Benzene[b]	0.67	-
Ag(111)-Benzene[d]	0.87	0.56[7]

[a] TZP basis sets were use for all of the atoms; [b] Slab contained 74 atoms; [c] Slab contained 134 atoms; [d] Slab contained 64 atoms.

The differences between the charge densities of the isolated fragments and that of the metal-adsorbate system were calculated. In the charge density difference (CDD) isosurfaces provided herein, red denotes a gain of electrons, and blue a loss of electrons upon adsorption. Charge density difference isosurfaces were calculated for the **S3** and **S5** structures (Figures 2a and 2b).

Figure 2b is illustrative of the "Pillow Effect", which is caused by Pauli repulsion between the metal and adsorbate electron densities[12]. The charge redistribution is also a result of electron donation from the HOMO of benzene to the metal surface, and back-donation from the surface to the benzene LUMO (the Dewar, Chatt, and Duncason model which has, for example, been applied to benzene on Cu(110)[13]). A Mulliken analysis illustrates that for both **S3** and **S5** there is a charge transfer of 0.19e to the metal cluster, whereas the Hirschfeld scheme yields 0.16e, and 0.27e for Ag(111) and Cu(111), respectively. Mulliken charges are strongly basis set dependent, and the Hirschfeld method may provide results which are more in-line with chemical intuition since the promolecular fragments are the same as those employed in our CDD calculations. The benzene to Ag/Cu surface distance was found to be 3.84/2.76 angstroms. The closer the adsorbate is to the metal, the stronger the binding energy and the more pronounced is the CDD.

Figure 2: Charge density difference (CDD) isosurfaces of benzene on an: (a) Ag(111) (**S3**), and (b) Cu(111) slab (**S5**). The slabs contained 64 atoms and the isovalues are +/- 0.0003 au.

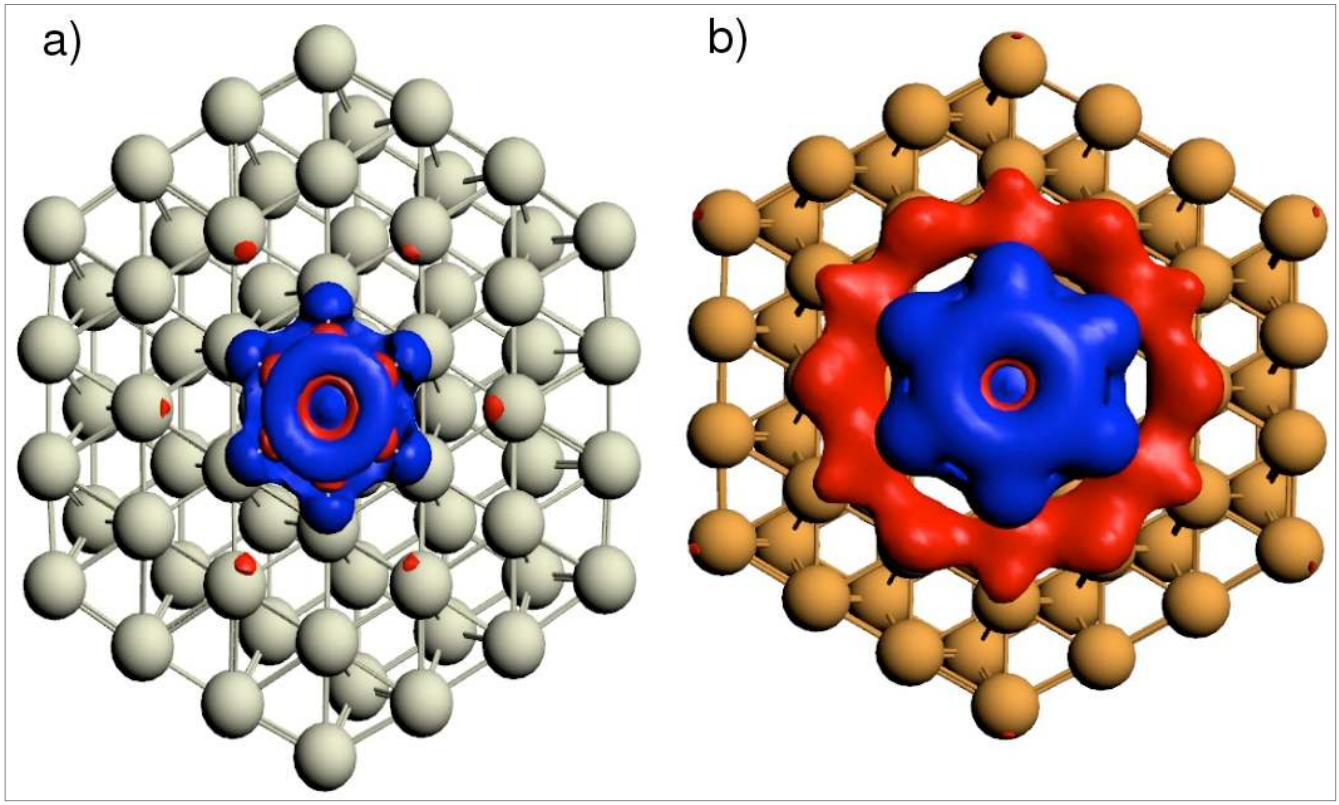

Section 4: Cu(111)/2H-TPP and Ag(111)/2H-TPP

Geometry optimizations were performed as previously described in Section 1, with the Cu(111) and Ag(111) clusters both containing 166 atoms. The coordinates of the following systems can be found in Section 5, and the BE are given in Table 3.

Table 3: Binding energies (BE) and structural parameters of 2H-TPP with Cu(111) and Ag(111)[a]

System	BE (eV)[b]	Surface Charge (Mulliken)	Surface Charge (Hirschfeld)	Dihedral	N1-surface Distance (Å)	N2-Surface Distance (Å)
Cu(111)	6.19/5.31	-1.69e	-0.89e	38.3	3.05	3.05
Ag(111)	3.44/3.07	-1.45e	-0.46e	42.1	3.30	3.29

[a] The atoms C1, C2, C3 and C4 which define the dihedral angle given are illustrated in Figure 3. The N1 and N2 atoms are defined in Figure 3.

[b] The uncorrected/BSSE corrected binding energies.

Figure 3: The carbon atoms which define the dihedral angle, and the nitrogen atoms given in Table 3.

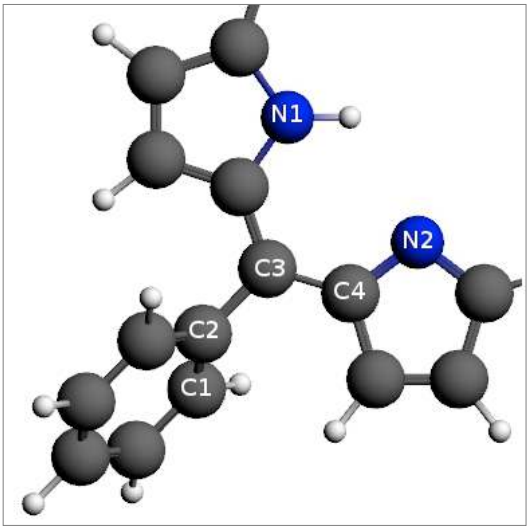

Figure 4: Charge density difference (CDD) isosurfaces of 2H-TPP on an: (a) Cu(111) (**S6**), and (b) Ag(111) slab (**S7**). The slabs contained 166 atoms and the isovalues are +/- 0.0003 au.

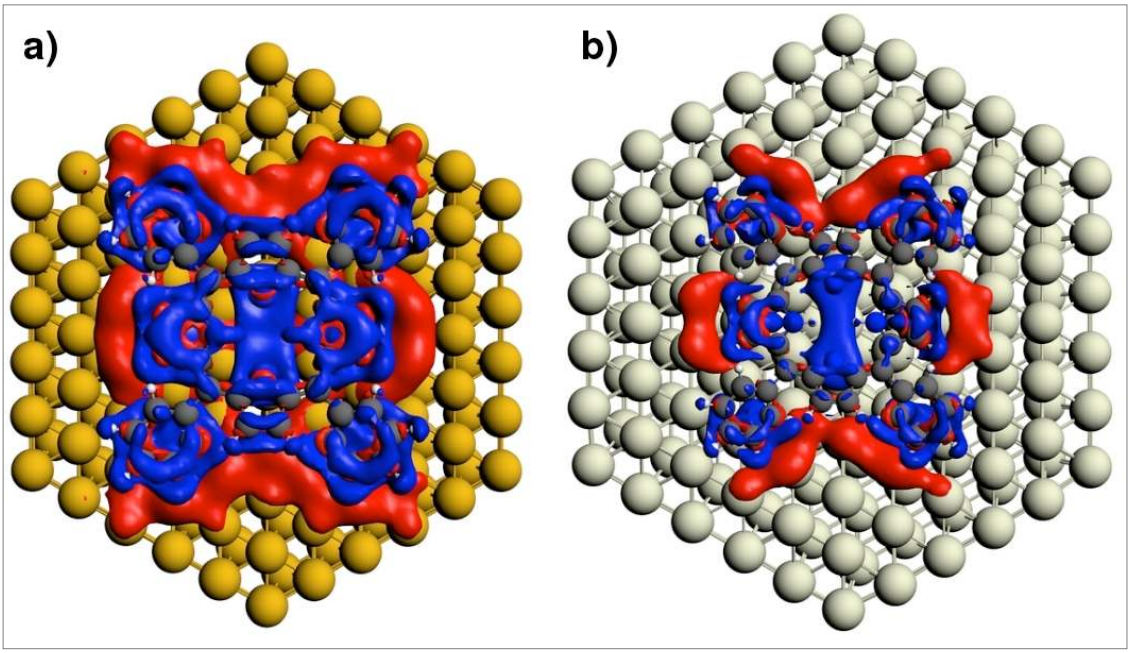

Table 4: Bonding Energy (eV) decomposition analysis for 2H-TPP on Cu(111) and Ag(111).

System	Pauli	Electrostatic	Steric Interaction	Orbital Interaction	Dispersion	Geometric Distortion
Cu(111)	15.27	-7.84	7.43	-5.07	-9.15	0.62
Ag(111	8.60	-4.44	4.16	-2.36	-5.70	0.53

)						

The 2H-TPP molecule distorts as it approaches the Cu(111) and Ag(111) surfaces. The phenyl arms rotate so that the dihedral angle, as defined in Figure 3, changes (for free 2H-TPP we compute the dihedral angle to be 62.7 degrees). In both cases the phenyl arms are oriented nearly parallel to the metal surface, with an angle of 26/30 degrees to Cu(111)/Ag(111). The ends of the pyrrole rings that contain N1 distort downwards, and the pyrrole rings that contain N2 distort upwards due to the rotation of the phenyl arms of the 2H-TPP.

In accordance with our findings for benzene on Ag(111)/Cu(111), the Mulliken charges for the two systems were about the same even though visual inspection of the CDD (Figures 4 and 5) appears to indicate a larger charge redistribution and charge build-up on the Cu surface. The Hirschfeld charge analysis, on the other hand, shows that there is a larger amount of charge transferred to Cu(111) than to Ag(111) suggesting that the repulsion between the positively charged 2H-TPP molecules may hinder their self-assembly. It is likely that the Hirschfeld scheme provides better results for the systems we are considering[19].

The BSSE uncorrected bonding energy can be decomposed as[14]:

$$BE = DE_{bond} = DE_{geo} + DE_{steric} + DE_{oi} + DE_{disp} \quad (2)$$

where DE_{geo} is the energy necessary to distort the geometry of the 2H-TPP to the one in the total system, DE_{steric}, the steric repulsion, is a sum of the Pauli repulsion and the classical electrostatic interaction between the interpenetrating charge densities of the fragments, DE_{oi} is the orbital interaction and DE_{disp} the dispersion energy. These values are provided in Table 4.

The distances between N1 and N2 and the metal surface is larger for the Ag(111) than for the Cu(111) slab, and the resulting charge redistribution upon absorption is smaller as evidenced in Figures 4 and 5. The stronger adsorbate-metal interaction for the Cu(111) system correlates with the larger magnitude of the steric, orbital and dispersion interaction energies, and the larger energy necessary to distort the 2H-TPP molecule as it adsorbs to the metal surface.

To clarify the nature of the bonding between 2H-TPP and Cu(111)/Ag(111), we calculated the composition of the molecular orbitals (MOs) in terms of the occupied and unoccupied MOs of the molecule and the metal cluster. Based upon the results of this analysis approximate interaction diagrams, provided in Fig. 6, can be constructed using the thinking outlined in Refs. [15-18].

These diagrams illustrate that the bonding is similar to benzene, with charge transfer from the 2H-TPP HOMO to the surface, and back donation into the 2H-TPP LUMO. Because of the shorter metal-adsorbate distance, the dispersion of the HOMO/metal and LUMO/metal bands is larger for Cu(111). The calculation of the crystal orbital overlap population (COOP) would be necessary for a more in-depth analysis of the bonding in the two systems.

Figure 5: Charge density difference (CDD) contours of 2H-TPP on an: (a) Cu(111) (**S6**), and (b) Ag(111) slab (**S7**). The slabs contained 166 atoms, and the settings used to obtain the contours in both plots was the same.

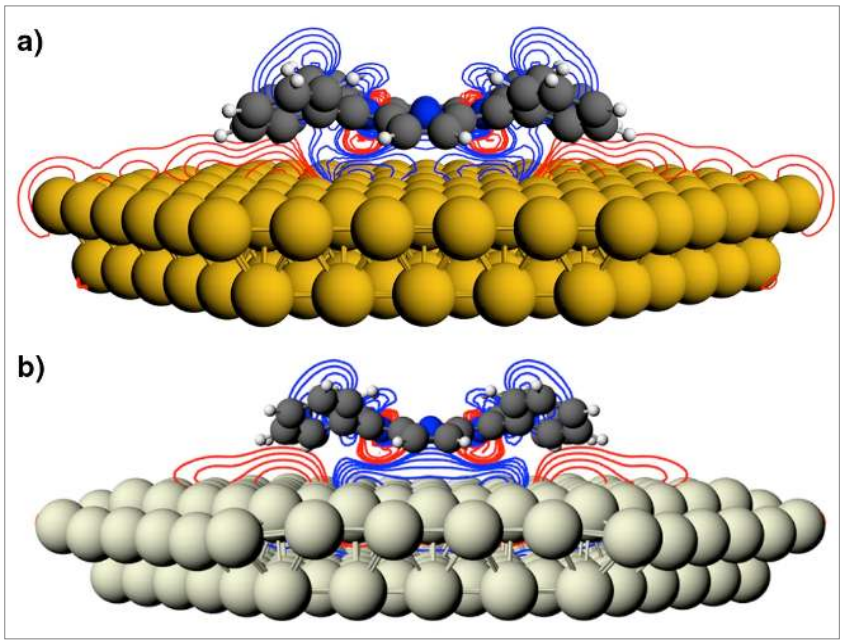

Figure 6: Schematic interaction diagram of 2H-TPP with the a) Ag(111) and b) Cu(111) surface. The Fermi level has been set to zero. Isosurfaces of the HOMO and LUMO of the 2H-TPP molecule (+/- 0.03 a.u.) are displayed in red/pink and green/yellow. The blue/red rectangles represent the width of the bands formed from the overlap of metal bands with the 2H-TPP HOMO/LUMO. On Cu some of the metal/LUMO bands are off the scale of this figure, as denoted by the dashed line. Note that the bandwidths of the metals extend to higher/lower energies.

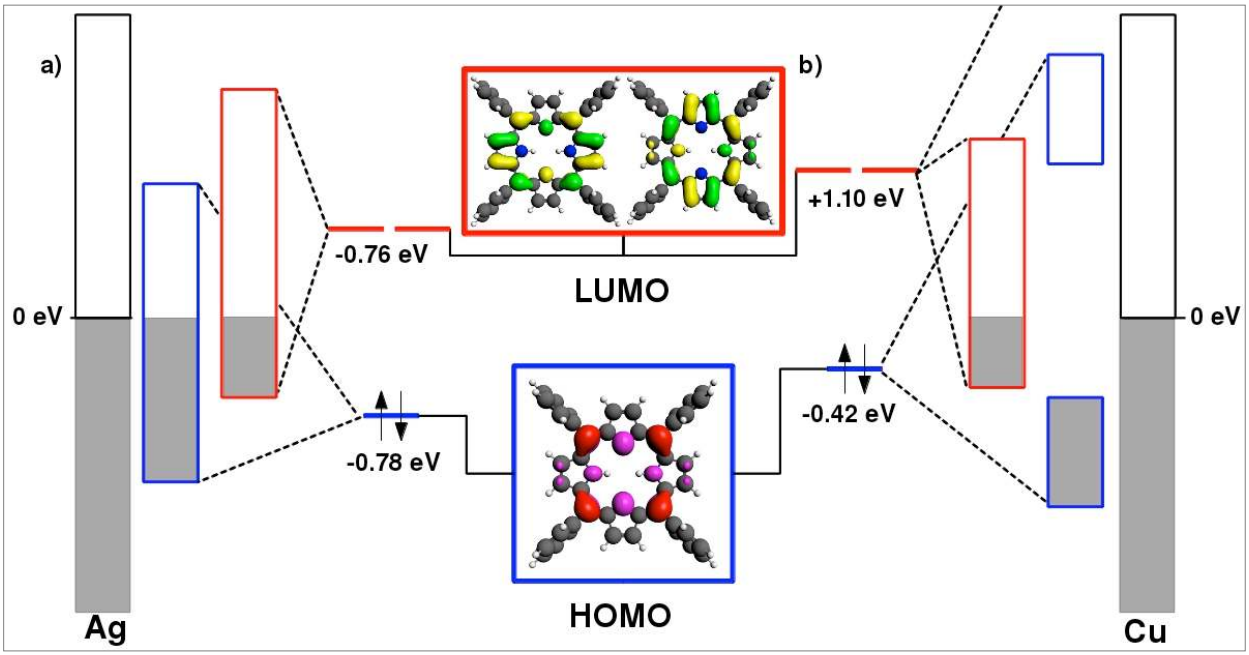
a)
b)
0 eV
0 eV
-0.76 eV
+1.10 eV
LUMO
-0.78 eV
-0.42 eV
HOMO
Ag
Cu

Section 5: Coordinates

S1-Adjacent 2H-TPP Dimer

E= -1043.98775848 eV Symmetry: C_{2v}

H	-14.632016	-6.294225	0.013682
H	-14.632016	6.294225	0.013682
C	-13.855608	-5.525492	0.006242
C	-13.855608	5.525492	0.006242
H	-13.467074	1.347669	0.173646
H	-13.467074	-1.347669	0.173646
H	-14.458660	-4.700141	-1.906099
H	-14.458660	4.700141	-1.906099
C	-13.759877	-4.629054	-1.069030
C	-13.759877	4.629054	-1.069030
C	-12.947725	-5.428541	1.071674
C	-12.947725	5.428541	1.071674
H	-13.017334	-6.119126	1.915801
H	-13.017334	6.119126	1.915801
C	-12.609272	-0.688133	0.091867
C	-12.609272	0.688133	0.091867
H	-12.686374	-2.943943	-1.912285
H	-12.686374	2.943943	-1.912285
C	-12.764706	-3.642393	-1.076429
C	-12.764706	3.642393	-1.076429
C	-11.952706	-4.441989	1.061912
C	-11.952706	4.441989	1.061912
H	-11.246395	-4.362053	1.890813
H	-11.246395	4.362053	1.890813
C	-11.848226	-3.535428	-0.012034
C	-11.848226	3.535428	-0.012034
C	-11.246159	1.136555	-0.005931
C	-11.246159	-1.136555	-0.005931
C	-10.791091	-2.472192	-0.016819
C	-10.791091	2.472192	-0.016819
N	-10.462042	0.000000	-0.060579
H	-9.683937	-5.131056	-0.226769
H	-9.683937	5.131056	-0.226769
H	-9.444133	0.000000	-0.071925
C	-9.432382	-2.875554	-0.027725
C	-9.432382	2.875554	-0.027725
C	-9.018772	-4.277214	-0.133434
C	-9.018772	4.277214	-0.133434
N	-8.339417	-2.041025	0.030416
N	-8.339417	2.041025	0.030416
C	-7.657112	-4.276954	-0.123939
C	-7.657112	4.276954	-0.123939
C	-7.245578	-2.875124	-0.015566
C	-7.245578	2.875124	-0.015566
H	-7.234471	0.000000	-0.048785
H	-6.990332	-5.130155	-0.207176
H	-6.990332	5.130155	-0.207176
N	-6.216737	0.000000	-0.035577
C	-5.887630	-2.471290	0.006142
C	-5.887630	2.471290	0.006142
C	-5.432601	-1.136302	0.017972
C	-5.432601	1.136302	0.017972
C	-4.829672	-3.534150	0.021180
C	-4.829672	3.534150	0.021180
H	-4.003367	-2.972578	-1.892724
H	-4.003367	2.972578	-1.892724
C	-3.920522	-3.658534	-1.047367
C	-3.920522	3.658534	-1.047367
C	-4.717910	-4.421836	1.109777
C	-4.717910	4.421836	1.109777
H	-5.417917	-4.327169	1.943165
H	-5.417917	4.327169	1.943165
C	-4.069503	-0.688135	0.114180
C	-4.069503	0.688135	0.114180
H	-2.234924	-4.731537	-1.872802
H	-2.234924	4.731537	-1.872802
C	-2.925351	-4.645308	-1.030518
C	-2.925351	4.645308	-1.030518
C	-3.722170	-5.407772	1.129407
C	-3.722170	5.407772	1.129407
H	-3.646927	-6.083479	1.984453
H	-3.646927	6.083479	1.984453
H	-3.212139	-1.347942	0.193526
H	-3.212139	1.347942	0.193526
C	-2.821721	-5.522984	0.059285
C	-2.821721	5.522984	0.059285
H	-2.044879	-6.291260	0.075238
H	-2.044879	6.291260	0.075238
H	2.044879	-6.291260	0.075238
H	2.044879	6.291260	0.075238
C	2.821721	-5.522984	0.059285
C	2.821721	5.522984	0.059285
H	3.212139	1.347942	0.193526
H	3.212139	-1.347942	0.193526
H	3.646927	-6.083479	1.984453
H	3.646927	6.083479	1.984453
C	3.722170	-5.407772	1.129407
C	3.722170	5.407772	1.129407
C	2.925351	-4.645308	-1.030518
C	2.925351	4.645308	-1.030518
H	2.234924	-4.731537	-1.872802
H	2.234924	4.731537	-1.872802
C	4.069503	-0.688135	0.114180

C	4.069503	0.688135	0.114180
H	5.417917	-4.327169	1.943165
H	5.417917	4.327169	1.943165
C	4.717910	-4.421836	1.109777
C	4.717910	4.421836	1.109777
C	3.920522	-3.658534	-1.047367
C	3.920522	3.658534	-1.047367
H	4.003367	-2.972578	-1.892724
H	4.003367	2.972578	-1.892724
C	4.829672	-3.534150	0.021180
C	4.829672	3.534150	0.021180
C	5.432601	1.136302	0.017972
C	5.432601	-1.136302	0.017972
C	5.887630	-2.471290	0.006142
C	5.887630	2.471290	0.006142
N	6.216737	0.000000	-0.035577
H	6.990332	-5.130155	-0.207176
H	6.990332	5.130155	-0.207176
H	7.234471	0.000000	-0.048785
C	7.245578	-2.875124	-0.015566
C	7.245578	2.875124	-0.015566
C	7.657112	-4.276954	-0.123939
C	7.657112	4.276954	-0.123939
N	8.339417	-2.041025	0.030416
N	8.339417	2.041025	0.030416
C	9.018772	-4.277214	-0.133434
C	9.018772	4.277214	-0.133434
C	9.432382	-2.875554	-0.027725
C	9.432382	2.875554	-0.027725
H	9.444133	0.000000	-0.071925
H	9.683937	-5.131056	-0.226769
H	9.683937	5.131056	-0.226769
N	10.462042	0.000000	-0.060579
C	10.791091	-2.472192	-0.016819
C	10.791091	2.472192	-0.016819
C	11.246159	-1.136555	-0.005931
C	11.246159	1.136555	-0.005931
C	11.848226	-3.535428	-0.012034
C	11.848226	3.535428	-0.012034
H	11.246395	-4.362053	1.890813
H	11.246395	4.362053	1.890813
C	11.952706	-4.441989	1.061912
C	11.952706	4.441989	1.061912
C	12.764706	-3.642393	-1.076429
C	12.764706	3.642393	-1.076429
H	12.686374	-2.943943	-1.912285
H	12.686374	2.943943	-1.912285
C	12.609272	-0.688133	0.091867
C	12.609272	0.688133	0.091867
H	13.017334	-6.119126	1.915801
H	13.017334	6.119126	1.915801
C	12.947725	-5.428541	1.071674
C	12.947725	5.428541	1.071674
C	13.759877	-4.629054	-1.069030
C	13.759877	4.629054	-1.069030
H	14.458660	-4.700141	-1.906099
H	14.458660	4.700141	-1.906099
H	13.467074	-1.347669	0.173646
H	13.467074	1.347669	0.173646
C	13.855608	-5.525492	0.006242
C	13.855608	5.525492	0.006242
H	14.632016	-6.294225	0.013682
H	14.632016	6.294225	0.013682

S2- Sandwich 2H-TPP Dimer

E= -1045.07165541 eV

C	-3.038613	2.742607	2.470483
C	-3.454285	2.946468	1.136601
C	-1.755541	2.275154	2.858180
C	-4.680716	3.547237	0.688350
C	-4.680716	3.547237	-0.688350
C	-3.454285	2.946468	-1.136601
C	-1.408678	1.930655	4.238644
C	-0.078398	1.640462	4.236598
C	0.376962	1.793599	2.852954
N	-2.744497	2.610311	0.000000
H	-1.788008	2.258651	0.000000
H	-5.444064	3.949786	1.345137
H	-5.444064	3.949786	-1.345137
N	-0.669077	2.131529	2.025456
H	-2.102342	1.874004	5.072249
H	0.534698	1.304006	5.066791
C	-3.038613	2.742607	-2.470483
C	-1.755541	2.275154	-2.858180
C	-1.408678	1.930655	-4.238644
C	-0.078398	1.640462	-4.236598
C	0.376962	1.793599	-2.852954
N	-0.669077	2.131529	-2.025456
H	-2.102342	1.874004	-5.072249
H	0.534698	1.304006	-5.066791
C	1.736363	1.648687	2.470138
C	3.564553	1.554078	0.688244
C	3.564553	1.554078	-0.688244
C	2.199121	1.587706	-1.137443
N	1.413468	1.589976	0.000000
H	4.427035	1.556618	-1.345752
C	1.736363	1.648687	-2.470138
C	2.199121	1.587706	1.137443

H	4.427035	1.556618	1.345752
H	0.404131	1.729419	0.000000
C	2.763464	1.650481	3.559518
C	2.800249	2.722829	4.477910
C	3.707615	0.614939	3.702444
C	3.747391	2.755301	5.509187
C	4.652626	0.643506	4.736032
C	4.677560	1.713133	5.643185
H	2.076016	3.533050	4.371231
H	3.675845	-0.224072	3.009162
H	3.760503	3.597021	6.205896
H	5.355845	-0.183454	4.843673
H	5.413832	1.731833	6.450847
C	2.763464	1.650481	-3.559518
C	2.800249	2.722829	-4.477910
C	3.707615	0.614939	-3.702444
C	3.747391	2.755301	-5.509187
C	4.652626	0.643506	-4.736032
C	4.677560	1.713133	-5.643185
H	2.076016	3.533050	-4.371231
H	3.675845	-0.224072	-3.009162
H	3.760503	3.597021	-6.205896
H	5.355845	-0.183454	-4.843673
H	5.413832	1.731833	-6.450847
C	-4.023894	3.090569	3.541163
C	-3.677966	3.997679	4.565595
C	-5.322581	2.541491	3.549994
C	-4.595642	4.335700	5.567857
C	-6.243284	2.879216	4.549526
C	-5.883016	3.776958	5.565822
H	-2.681423	4.443954	4.560140
H	-5.600958	1.834475	2.767149
H	-4.306953	5.045377	6.346558
H	-7.240827	2.433855	4.539081
H	-6.599639	4.042275	6.346667
C	-4.023894	3.090569	-3.541163
C	-3.677966	3.997679	-4.565595
C	-5.322581	2.541491	-3.549994
C	-4.595642	4.335700	-5.567857
C	-6.243284	2.879216	-4.549526
C	-5.883016	3.776958	-5.565822
H	-2.681423	4.443954	-4.560140
H	-5.600958	1.834475	-2.767149
H	-4.306953	5.045377	-6.346558
H	-7.240827	2.433855	-4.539081
H	-6.599639	4.042275	-6.346667
C	-1.736363	-1.648687	2.470138
C	-2.199121	-1.587706	1.137443
C	-0.376962	-1.793599	2.852954
C	-3.564553	-1.554078	0.688244
C	-3.564553	-1.554078	-0.688244
C	-2.199121	-1.587706	-1.137443
C	0.078398	-1.640462	4.236598
C	1.408678	-1.930655	4.238644
C	1.755541	-2.275154	2.858180
N	-1.413468	-1.589976	0.000000
H	-0.404131	-1.729419	0.000000
H	-4.427035	-1.556618	1.345752
H	-4.427035	-1.556618	-1.345752
N	0.669077	-2.131529	2.025456
H	-0.534698	-1.304006	5.066791
H	2.102342	-1.874004	5.072249
C	-1.736363	-1.648687	-2.470138
C	-0.376962	-1.793599	-2.852954
C	0.078398	-1.640462	-4.236598
C	1.408678	-1.930655	-4.238644
C	1.755541	-2.275154	-2.858180
N	0.669077	-2.131529	-2.025456
H	-0.534698	-1.304006	-5.066791
H	2.102342	-1.874004	-5.072249
C	3.038613	-2.742607	2.470483
C	4.680716	-3.547237	0.688350
C	4.680716	-3.547237	-0.688350
C	3.454285	-2.946468	-1.136601
N	2.744497	-2.610311	0.000000
H	5.444064	-3.949786	-1.345137
C	3.038613	-2.742607	-2.470483
C	3.454285	-2.946468	1.136601
H	5.444064	-3.949786	1.345137
H	1.788008	-2.258651	0.000000
C	4.023894	-3.090569	3.541163
C	5.322581	-2.541491	3.549994
C	3.677966	-3.997679	4.565595
C	6.243284	-2.879216	4.549526
C	4.595642	-4.335700	5.567857
C	5.883016	-3.776958	5.565822
H	5.600958	-1.834475	2.767149
H	2.681423	-4.443954	4.560140
H	7.240827	-2.433855	4.539081
H	4.306953	-5.045377	6.346558
H	6.599639	-4.042275	6.346667
C	4.023894	-3.090569	-3.541163
C	5.322581	-2.541491	-3.549994
C	3.677966	-3.997679	-4.565595
C	6.243284	-2.879216	-4.549526
C	4.595642	-4.335700	-5.567857
C	5.883016	-3.776958	-5.565822
H	5.600958	-1.834475	-2.767149

H	2.681423	-4.443954	-4.560140
H	7.240827	-2.433855	-4.539081
H	4.306953	-5.045377	-6.346558
H	6.599639	-4.042275	-6.346667
C	-2.763464	-1.650481	3.559518
C	-3.707615	-0.614939	3.702444
C	-2.800249	-2.722829	4.477910
C	-4.652626	-0.643506	4.736032
C	-3.747391	-2.755301	5.509187
C	-4.677560	-1.713133	5.643185
H	-3.675845	0.224072	3.009162
H	-2.076016	-3.533050	4.371231
H	-5.355845	0.183454	4.843673
H	-3.760503	-3.597021	6.205896
H	-5.413832	-1.731833	6.450847
C	-2.763464	-1.650481	-3.559518
C	-3.707615	-0.614939	-3.702444
C	-2.800249	-2.722829	-4.477910
C	-4.652626	-0.643506	-4.736032
C	-3.747391	-2.755301	-5.509187
C	-4.677560	-1.713133	-5.643185
H	-3.675845	0.224072	-3.009162
H	-2.076016	-3.533050	-4.371231
H	-5.355845	0.183454	-4.843673
H	-3.760503	-3.597021	-6.205896
H	-5.413832	-1.731833	-6.450847

S3- Ag(111)_64-Benzene

E=-183.74769746 eV Symmetry: C_{3v}

Ag	-6.672409	2.889236	-1.293224
Ag	-6.672409	-2.889236	-1.293224
Ag	5.838356	-4.333857	-1.293224
Ag	5.838356	4.333857	-1.293224
Ag	0.834052	-7.223094	-1.293224
Ag	0.834052	7.223094	-1.293224
Ag	-6.672411	0.000000	-1.293222
Ag	3.336206	-5.778478	-1.293222
Ag	3.336206	5.778478	-1.293222
Ag	-4.170257	1.444622	-1.293220
Ag	-4.170257	-1.444622	-1.293220
Ag	3.336207	-2.889238	-1.293220
Ag	3.336207	2.889238	-1.293220
Ag	0.834049	-4.333859	-1.293220
Ag	0.834049	4.333859	-1.293220
Ag	-1.668100	0.000000	-1.293216
Ag	0.834050	-1.444617	-1.293216
Ag	0.834050	1.444617	-1.293216
Ag	-1.668102	-2.889237	-1.293214
Ag	-1.668102	2.889237	-1.293214
Ag	3.336203	0.000000	-1.293214
Ag	-1.668100	-5.778479	-1.293212
Ag	-1.668100	5.778479	-1.293212
Ag	-4.170260	-4.333857	-1.293212
Ag	-4.170260	4.333857	-1.293212
Ag	5.838360	1.444622	-1.293212
Ag	5.838360	-1.444622	-1.293212
Ag	-7.787319	4.597414	0.982917
Ag	-7.787319	-4.597414	0.982917
Ag	7.875137	-4.445310	0.982917
Ag	7.875137	4.445310	0.982917
Ag	-0.087817	-9.042723	0.982917
Ag	-0.087817	9.042723	0.982917
Ag	-7.954438	1.518828	1.202254
Ag	-7.954438	-1.518828	1.202254
Ag	5.292563	-6.129331	1.202254
Ag	5.292563	6.129331	1.202254
Ag	2.661875	-7.648160	1.202254
Ag	2.661875	7.648160	1.202254
Ag	-5.248020	3.062867	1.676706
Ag	-5.248020	-3.062867	1.676706
Ag	5.276530	-3.013485	1.676706
Ag	5.276530	3.013485	1.676706
Ag	-0.028511	-6.076352	1.676706
Ag	-0.028511	6.076352	1.676706
Ag	-5.295288	0.000000	1.665041
Ag	2.647644	-4.585854	1.665041
Ag	2.647644	4.585854	1.665041
Ag	-2.699858	1.561404	1.468911
Ag	-2.699858	-1.561404	1.468911
Ag	2.702144	-1.557444	1.468911
Ag	2.702144	1.557444	1.468911
Ag	-0.002286	-3.118847	1.468911
Ag	-0.002286	3.118847	1.468911
Ag	-2.651321	-4.592222	1.669296
Ag	-2.651321	4.592222	1.669296
Ag	5.302642	0.000000	1.669296
Ag	0.000000	0.000000	1.312384
Ag	-2.721867	-7.678530	0.691063
Ag	-2.721867	7.678530	0.691063
Ag	-5.288869	-6.196471	0.691063
Ag	-5.288869	6.196471	0.691063
Ag	8.010735	1.482059	0.691063
Ag	8.010735	-1.482059	0.691063
C	-1.217347	0.702723	4.528152
C	-1.217347	-0.702723	4.528152

C	0.000098	-1.405615	4.528152
C	1.217250	-0.702892	4.528152
C	1.217250	0.702892	4.528152
C	0.000098	1.405615	4.528152
H	-2.163502	1.249690	4.528808
H	-2.163502	-1.249690	4.528808
H	-0.000512	-2.498492	4.528808
H	2.164014	-1.248802	4.528808
H	2.164014	1.248802	4.528808
H	-0.000512	2.498492	4.528808

S4- Ag(111)_166-Benzene

E=-372.89129933 eV Symmetry: C_{3v}

Ag	-0.834052	1.444620	-1.641278
Ag	-0.834052	-1.444620	-1.641278
Ag	1.668103	0.000000	-1.641278
Ag	-0.834055	10.112322	-1.641277
Ag	-8.340500	5.778474	-1.641277
Ag	-0.834055	-10.112322	-1.641277
Ag	9.174555	-4.333848	-1.641277
Ag	-8.340500	-5.778474	-1.641277
Ag	9.174555	4.333848	-1.641277
Ag	-0.834054	4.333856	-1.641274
Ag	-3.336202	2.889240	-1.641274
Ag	-0.834054	-4.333856	-1.641274
Ag	4.170256	-1.444616	-1.641274
Ag	-3.336202	-2.889240	-1.641274
Ag	4.170256	1.444616	-1.641274
Ag	-0.834054	13.001559	-1.641274
Ag	-10.842654	7.223092	-1.641274
Ag	-0.834054	-13.001559	-1.641274
Ag	11.676708	-5.778467	-1.641274
Ag	-10.842654	-7.223092	-1.641274
Ag	11.676708	5.778467	-1.641274
Ag	-3.336213	8.667703	-1.641273
Ag	-5.838345	7.223097	-1.641273
Ag	-3.336213	-8.667703	-1.641273
Ag	9.174558	-1.444606	-1.641273
Ag	-5.838345	-7.223097	-1.641273
Ag	9.174558	1.444606	-1.641273
Ag	-0.834054	7.223084	-1.641271
Ag	-5.838348	4.333854	-1.641271
Ag	-0.834054	-7.223084	-1.641271
Ag	6.672402	-2.889230	-1.641271
Ag	-5.838348	-4.333854	-1.641271
Ag	6.672402	2.889230	-1.641271
Ag	-3.336203	11.556930	-1.641269
Ag	-8.340494	8.667702	-1.641269
Ag	-3.336203	-11.556930	-1.641269
Ag	11.676697	-2.889229	-1.641269
Ag	-8.340494	-8.667702	-1.641269
Ag	11.676697	2.889229	-1.641269
Ag	-3.336206	5.778479	-1.641266
Ag	-3.336206	-5.778479	-1.641266
Ag	6.672412	0.000000	-1.641266
Ag	-5.838351	10.112321	-1.641265
Ag	-5.838351	-10.112321	-1.641265
Ag	11.676702	0.000000	-1.641265
Ag	-3.336201	0.000000	-1.641263
Ag	1.668100	2.889235	-1.641263
Ag	1.668100	-2.889235	-1.641263
Ag	-5.838359	-1.444619	-1.641259
Ag	4.170256	4.333858	-1.641259
Ag	-5.838359	1.444619	-1.641259
Ag	1.668103	5.778477	-1.641259
Ag	4.170256	-4.333858	-1.641259
Ag	1.668103	-5.778477	-1.641259
Ag	-8.340507	-2.889239	-1.641254
Ag	6.672408	5.778472	-1.641254
Ag	-8.340507	2.889239	-1.641254
Ag	1.668099	8.667711	-1.641254
Ag	6.672408	-5.778472	-1.641254
Ag	1.668099	-8.667711	-1.641254
Ag	-8.340507	0.000000	-1.641251
Ag	4.170254	7.223091	-1.641251
Ag	4.170254	-7.223091	-1.641251
Ag	-10.842655	-4.333848	-1.641250
Ag	9.174550	7.223091	-1.641250
Ag	-10.842655	4.333848	-1.641250
Ag	1.668105	11.556939	-1.641250
Ag	9.174550	-7.223091	-1.641250
Ag	1.668105	-11.556939	-1.641250
Ag	-10.842656	-1.444620	-1.641246
Ag	6.672406	8.667705	-1.641246
Ag	-10.842656	1.444620	-1.641246
Ag	4.170250	10.112325	-1.641246
Ag	6.672406	-8.667705	-1.641246
Ag	4.170250	-10.112325	-1.641246
Ag	-13.132014	-4.667425	0.240009
Ag	10.608116	9.038945	0.240009
Ag	-13.132014	4.667425	0.240009
Ag	2.523898	13.706371	0.240009
Ag	10.608116	-9.038945	0.240009
Ag	2.523898	-13.706371	0.240009
Ag	-13.079773	-1.593239	0.297832
Ag	7.919671	10.530796	0.297832
Ag	-13.079773	1.593239	0.297832
Ag	5.160101	12.124035	0.297832

Ag	7.919671	-10.530796	0.297832
Ag	5.160101	-12.124035	0.297832
Ag	-0.094487	15.172654	0.487307
Ag	-13.092660	7.668155	0.487307
Ag	-0.094487	-15.172654	0.487307
Ag	13.187147	-7.504499	0.487307
Ag	-13.092660	-7.668155	0.487307
Ag	13.187147	7.504499	0.487307
Ag	-5.417787	12.383932	0.676159
Ag	-8.015906	10.883907	0.676159
Ag	-5.417787	-12.383932	0.676159
Ag	13.433693	-1.500025	0.676159
Ag	-8.015906	-10.883907	0.676159
Ag	13.433693	1.500025	0.676159
Ag	-2.810427	13.837082	0.730460
Ag	-10.578051	9.352442	0.730460
Ag	-2.810427	-13.837082	0.730460
Ag	13.388478	-4.484640	0.730460
Ag	-10.578051	-9.352442	0.730460
Ag	13.388478	4.484640	0.730460
Ag	0.000000	0.000000	1.023508
Ag	-0.005871	3.057964	1.132958
Ag	-2.645339	1.534066	1.132958
Ag	-0.005871	-3.057964	1.132958
Ag	2.651209	-1.523898	1.132958
Ag	-2.645339	-1.534066	1.132958
Ag	2.651209	1.523898	1.132958
Ag	-5.257672	0.000000	1.198300
Ag	2.628836	4.553278	1.198300
Ag	2.628836	-4.553278	1.198300
Ag	-2.672926	7.669849	1.194878
Ag	-5.305821	6.149747	1.194878
Ag	-2.672926	-7.669849	1.194878
Ag	7.978747	-1.520102	1.194878
Ag	-5.305821	-6.149747	1.194878
Ag	7.978747	1.520102	1.194878
Ag	-0.036086	6.128158	1.203431
Ag	-5.289098	3.095331	1.203431
Ag	-0.036086	-6.128158	1.203431
Ag	5.325184	-3.032828	1.203431
Ag	-5.289098	-3.095331	1.203431
Ag	5.325184	3.032828	1.203431
Ag	-10.482963	0.000000	1.198702
Ag	5.241482	9.078512	1.198702
Ag	5.241482	-9.078512	1.198702
Ag	-5.312810	9.202056	1.192267
Ag	-5.312810	-9.202056	1.192267
Ag	10.625619	0.000000	1.192267
Ag	-2.650993	4.591655	1.212813
Ag	-2.650993	-4.591655	1.212813
Ag	5.301987	0.000000	1.212813
Ag	-0.044086	9.174546	1.224618
Ag	-7.923347	4.625453	1.224618
Ag	-0.044086	-9.174546	1.224618
Ag	7.967433	-4.549093	1.224618
Ag	-7.923347	-4.625453	1.224618
Ag	7.967433	4.549093	1.224618
Ag	-7.889211	-1.551838	1.235125
Ag	5.288537	6.056339	1.235125
Ag	-7.889211	1.551838	1.235125
Ag	2.600675	7.608176	1.235125
Ag	5.288537	-6.056339	1.235125
Ag	2.600675	-7.608176	1.235125
Ag	-10.508123	-3.094728	1.242239
Ag	7.934175	7.552937	1.242239
Ag	-10.508123	3.094728	1.242239
Ag	2.573948	10.647666	1.242239
Ag	7.934175	-7.552937	1.242239
Ag	2.573948	-10.647666	1.242239
Ag	-2.692265	10.736687	1.239069
Ag	-7.952111	7.699913	1.239069
Ag	-2.692265	-10.736687	1.239069
Ag	10.644376	-3.036774	1.239069
Ag	-7.952111	-7.699913	1.239069
Ag	10.644376	3.036774	1.239069
Ag	-0.070019	12.182003	1.297401
Ag	-10.514915	6.151640	1.297401
Ag	-0.070019	-12.182003	1.297401
Ag	10.584933	-6.030363	1.297401
Ag	-10.514915	-6.151640	1.297401
Ag	10.584933	6.030363	1.297401
C	0.000033	1.404795	4.281678
C	-1.216604	0.702369	4.281678
C	-1.216604	-0.702369	4.281678
C	0.000033	-1.404795	4.281678
C	1.216572	-0.702426	4.281678
C	1.216572	0.702426	4.281678
H	0.000240	2.497448	4.272639
H	-2.162974	1.248516	4.272639
H	-2.162974	-1.248516	4.272639
H	0.000240	-2.497448	4.272639
H	2.162734	-1.248932	4.272639
H	2.162734	1.248932	4.272639

S5- Cu(111)_64-Benzene

E= -232.05207362 eV Symmetry: C_{3v}

CU	-5.158257	-3.828868	2.032641
CU	-5.158257	3.828868	2.032641

CU	-0.736769	6.381616	2.032641
CU	-0.736769	-6.381616	2.032641
CU	5.895026	-2.552748	2.032641
CU	5.895026	2.552748	2.032641
CU	-0.736889	-1.276329	2.032520
CU	-0.736889	1.276329	2.032520
CU	1.473778	0.000000	2.032520
CU	-2.947539	5.105288	2.032512
CU	-2.947539	-5.105288	2.032512
CU	5.895078	0.000000	2.032512
CU	-2.947628	0.000000	2.032371
CU	1.473814	2.552721	2.032371
CU	1.473814	-2.552721	2.032371
CU	-2.947628	2.552669	2.032312
CU	-2.947628	-2.552669	2.032312
CU	-0.736862	3.829055	2.032312
CU	3.684490	1.276386	2.032312
CU	3.684490	-1.276386	2.032312
CU	-0.736862	-3.829055	2.032312
CU	-5.158207	-1.276329	2.032302
CU	-5.158207	1.276329	2.032302
CU	1.473770	5.105303	2.032302
CU	3.684437	3.828974	2.032302
CU	1.473770	-5.105303	2.032302
CU	3.684437	-3.828974	2.032302
CU	4.438931	-5.160010	0.025258
CU	2.249234	-6.424232	0.025258
CU	-6.688165	-1.264222	0.025258
CU	-6.688165	1.264222	0.025258
CU	2.249234	6.424232	0.025258
CU	4.438931	5.160010	0.025258
CU	6.603256	-3.830932	-0.073919
CU	0.016057	-7.634053	-0.073919
CU	-6.619312	-3.803121	-0.073919
CU	-6.619312	3.803121	-0.073919
CU	0.016057	7.634053	-0.073919
CU	6.603256	3.830932	-0.073919
CU	6.639379	1.270970	-0.116967
CU	6.639379	-1.270970	-0.116967
CU	-2.218997	-6.385356	-0.116967
CU	-4.420382	-5.114386	-0.116967
CU	-4.420382	5.114386	-0.116967
CU	-2.218997	6.385356	-0.116967
CU	0.000000	0.000000	-0.079687
CU	2.227987	-1.291122	-0.179093
CU	0.004151	-2.575054	-0.179093
CU	-2.232138	-1.283932	-0.179093
CU	-2.232138	1.283932	-0.179093
CU	0.004151	2.575054	-0.179093
CU	2.227987	1.291122	-0.179093
CU	2.221518	-3.847783	-0.224244
CU	-4.443037	0.000000	-0.224244
CU	2.221518	3.847783	-0.224244
CU	0.015427	-5.110435	-0.228404
CU	-4.433480	-2.541858	-0.228404
CU	-4.433480	2.541858	-0.228404
CU	0.015427	5.110435	-0.228404
CU	4.418053	2.568577	-0.228404
CU	4.418053	-2.568577	-0.228404
CU	-2.210259	-3.828281	-0.251616
CU	-2.210259	3.828281	-0.251616
CU	4.420518	0.000000	-0.251616
C	-1.219381	0.704528	-3.012385
C	-1.219381	-0.704528	-3.012385
C	-0.000449	-1.408279	-3.012385
C	1.219830	-0.703750	-3.012385
C	1.219830	0.703750	-3.012385
C	-0.000449	1.408279	-3.012385
H	-2.166704	1.250391	-2.989851
H	-2.166704	-1.250391	-2.989851
H	0.000482	-2.501616	-2.989851
H	2.166222	-1.251226	-2.989851
H	2.166222	1.251226	-2.989851
H	0.000482	2.501616	-2.989851

S6-Cu(111)-TPP

E=-957.51619907 eV Symmetry: C_s

Cu	8.105765	-1.142575	-6.381640
Cu	8.105765	-1.142575	6.381640
Cu	1.473780	-1.142575	-10.210618
Cu	1.473780	-1.142575	10.210618
Cu	-9.579545	-1.142575	3.828978
Cu	-9.579545	-1.142575	-3.828978
Cu	5.895106	-1.142573	-7.657965
Cu	5.895106	-1.142573	7.657965
Cu	3.684439	-1.142573	-8.934294
Cu	3.684439	-1.142573	8.934294
Cu	-9.579545	-1.142573	1.276329
Cu	-9.579545	-1.142573	-1.276329
Cu	5.895105	-1.142571	-5.105304
Cu	5.895105	-1.142571	5.105304
Cu	1.473770	-1.142571	-7.657963
Cu	1.473770	-1.142571	7.657963
Cu	-7.368876	-1.142571	2.552659
Cu	-7.368876	-1.142571	-2.552659
Cu	10.316433	-1.142569	5.105310
Cu	10.316433	-1.142569	-5.105310
Cu	3.684438	-1.142569	-6.381633

Cu	3.684438	-1.142569	6.381633
Cu	-0.736888	-1.142569	-11.486948
Cu	-0.736888	-1.142569	11.486948
Cu	-7.368876	-1.142569	0.000000
Cu	-9.579545	-1.142569	-6.381638
Cu	-9.579545	-1.142569	6.381638
Cu	3.684442	-1.142567	-3.828982
Cu	3.684442	-1.142567	3.828982
Cu	1.473774	-1.142567	-5.105311
Cu	1.473774	-1.142567	5.105311
Cu	-5.158216	-1.142567	1.276329
Cu	-5.158216	-1.142567	-1.276329
Cu	8.105764	-1.142566	3.828979
Cu	8.105764	-1.142566	-3.828979
Cu	-0.736889	-1.142566	-8.934287
Cu	-0.736889	-1.142566	8.934287
Cu	-7.368875	-1.142566	-5.105308
Cu	-7.368875	-1.142566	5.105308
Cu	10.316432	-1.142565	2.552650
Cu	10.316432	-1.142565	-2.552650
Cu	-2.947556	-1.142565	-10.210617
Cu	-2.947556	-1.142565	10.210617
Cu	-7.368876	-1.142565	-7.657967
Cu	-7.368876	-1.142565	7.657967
Cu	5.895101	-1.142564	-2.552657
Cu	5.895101	-1.142564	2.552657
Cu	-0.736884	-1.142564	-6.381636
Cu	-0.736884	-1.142564	6.381636
Cu	-5.158216	-1.142564	-3.828978
Cu	-5.158216	-1.142564	3.828978
Cu	8.105768	-1.142563	-1.276328
Cu	8.105768	-1.142563	1.276328
Cu	1.473774	-1.142563	-2.552651
Cu	1.473774	-1.142563	2.552651
Cu	-2.947547	-1.142563	0.000000
Cu	-2.947552	-1.142563	-7.657965
Cu	-2.947552	-1.142563	7.657965
Cu	-5.158216	-1.142563	-6.381637
Cu	-5.158216	-1.142563	6.381637
Cu	3.684441	-1.142562	-1.276321
Cu	3.684441	-1.142562	1.276321
Cu	-0.736894	-1.142562	-3.828980
Cu	-0.736894	-1.142562	3.828980
Cu	-2.947547	-1.142562	-2.552659
Cu	-2.947547	-1.142562	2.552659
Cu	10.316427	-1.142561	0.000000
Cu	-5.158214	-1.142561	-8.934288
Cu	-5.158214	-1.142561	8.934288
Cu	5.895100	-1.142560	0.000000
Cu	1.473778	-1.142560	0.000000
Cu	-0.736889	-1.142560	-1.276329
Cu	-0.736889	-1.142560	1.276329
Cu	-2.947550	-1.142560	-5.105306
Cu	-2.947550	-1.142560	5.105306
Cu	8.860490	0.957321	-7.663791
Cu	8.860490	0.957321	7.663791
Cu	2.206793	0.957321	-11.505305
Cu	2.206793	0.957321	11.505305
Cu	-11.067282	0.957321	3.841514
Cu	-11.067282	0.957321	-3.841514
Cu	6.643155	0.943229	-8.937935
Cu	6.643155	0.943229	8.937935
Cu	4.418901	0.943229	-10.222109
Cu	4.418901	0.943229	10.222109
Cu	-11.062056	0.943229	1.284174
Cu	-11.062056	0.943229	-1.284174
Cu	6.643226	1.063727	-6.378226
Cu	6.643226	1.063727	6.378226
Cu	2.202092	1.063727	-8.942316
Cu	2.202092	1.063727	8.942316
Cu	-8.845319	1.063727	2.564090
Cu	-8.845319	1.063727	-2.564090
Cu	11.063551	0.959830	6.377028
Cu	11.063551	0.959830	-6.377028
Cu	4.422871	1.063741	-7.660638
Cu	4.422871	1.063741	7.660638
Cu	-0.009107	0.959830	-12.769830
Cu	-0.009107	0.959830	12.769830
Cu	-8.845743	1.063741	0.000000
Cu	-11.054444	0.959830	-6.392802
Cu	-11.054444	0.959830	6.392802
Cu	4.424540	1.100325	-5.101812
Cu	4.424540	1.100325	5.101812
Cu	2.206028	1.100325	-6.382670
Cu	2.206028	1.100325	6.382670
Cu	-6.630569	1.100325	1.280858
Cu	-6.630569	1.100325	-1.280858
Cu	8.866523	1.085428	5.105915
Cu	8.866523	1.085428	-5.105915
Cu	-0.011409	1.085428	-10.231592
Cu	-0.011409	1.085428	10.231592
Cu	-8.855114	1.085428	-5.125676
Cu	-8.855114	1.085428	5.125676
Cu	11.105078	0.976411	3.825237
Cu	11.105078	0.976411	-3.825237
Cu	-2.239787	0.976411	-11.529898
Cu	-2.239787	0.976411	11.529898
Cu	-8.865291	0.976411	-7.704661

Cu	-8.865291	0.976411	7.704661
Cu	6.648332	1.090726	3.830177
Cu	6.648332	1.090726	-3.830177
Cu	-0.007135	1.090726	-7.672713
Cu	-0.007135	1.090726	7.672713
Cu	-6.641197	1.090726	-3.842536
Cu	-6.641197	1.090726	3.842536
Cu	2.209076	1.069521	-3.826233
Cu	2.209076	1.069521	3.826233
Cu	-4.418153	1.069521	0.000000
Cu	8.862277	1.105460	2.561247
Cu	8.862277	1.105460	-2.561247
Cu	4.441194	1.098855	-2.560546
Cu	4.441194	1.098855	2.560546
Cu	-0.003099	1.098855	-5.126460
Cu	-0.003099	1.098855	5.126460
Cu	-2.213034	1.105460	-8.955581
Cu	-2.213034	1.105460	8.955581
Cu	-4.438095	1.098855	-2.565914
Cu	-4.438095	1.098855	2.565914
Cu	-6.649244	1.105460	-6.394334
Cu	-6.649244	1.105460	6.394334
Cu	11.094578	0.983895	1.281284
Cu	11.094578	0.983895	-1.281284
Cu	-4.437664	0.983895	-10.248829
Cu	-4.437664	0.983895	10.248829
Cu	-6.656914	0.983895	-8.967544
Cu	-6.656914	0.983895	8.967544
Cu	6.644651	1.081595	-1.271261
Cu	6.644651	1.081595	1.271261
Cu	-2.221381	1.081595	-6.390067
Cu	-2.221381	1.081595	6.390067
Cu	-4.423270	1.081595	-5.118806
Cu	-4.423270	1.081595	5.118806
Cu	8.870651	1.101197	0.000000
Cu	2.218557	1.061629	-1.275808
Cu	2.218557	1.061629	1.275808
Cu	-0.004397	1.061629	-2.559231
Cu	-0.004397	1.061629	2.559231
Cu	-2.214160	1.061629	-1.283423
Cu	-2.214160	1.061629	1.283423
Cu	-4.435326	1.101197	-7.682209
Cu	-4.435326	1.101197	7.682209
Cu	4.430122	1.090351	0.000000
Cu	-2.215061	1.090351	-3.836598
Cu	-2.215061	1.090351	3.836598
Cu	0.000000	1.067131	0.000000
H	-2.033407	3.439537	-5.049510
H	-2.033407	3.439537	5.049510
H	2.413003	3.428917	-5.054629
H	2.413003	3.428917	5.054629
H	-3.680270	3.527812	-6.874598
H	-3.680270	3.527812	6.874598
H	4.080223	3.547983	-6.859862
H	4.080223	3.547983	6.859862
H	5.263510	3.498115	1.334079
H	5.263510	3.498115	-1.334079
H	-4.937082	3.505484	-1.330024
H	-4.937082	3.505484	1.330024
C	4.410758	3.693234	-0.694118
C	4.410758	3.693234	0.694118
C	-4.082799	3.707161	-0.693617
C	-4.082799	3.707161	0.693617
C	-3.018739	3.870888	-4.853508
C	-3.018739	3.870888	4.853508
C	3.390045	3.872533	-4.847142
C	3.390045	3.872533	4.847142
C	-3.960609	3.914886	-5.891039
C	-3.960609	3.914886	5.891039
C	4.343340	3.934985	-5.872117
C	4.343340	3.934985	5.872117
C	3.077207	3.996465	1.146630
C	3.077207	3.996465	-1.146630
C	-2.748589	4.004284	-1.147257
C	-2.748589	4.004284	1.147257
N	0.168513	4.113168	-2.054745
N	0.168513	4.113168	2.054745
N	2.305394	4.111571	0.000000
N	-1.976669	4.117776	0.000000
C	2.635935	4.264059	-2.471391
C	2.635935	4.264059	2.471391
C	-2.300769	4.271351	-2.470363
C	-2.300769	4.271351	2.470363
H	1.293361	4.231886	0.000000
H	-0.966019	4.246815	0.000000
C	1.267815	4.487450	-2.807675
C	-0.931175	4.496396	-2.802688
C	1.267815	4.487450	2.807675
C	-0.931175	4.496396	2.802688
C	-3.317766	4.364024	-3.558318
C	-3.317766	4.364024	3.558318
C	3.663740	4.370267	-3.547697
C	3.663740	4.370267	3.547697
C	-5.252599	4.409375	-5.657177
C	-5.252599	4.409375	5.657177
C	5.622124	4.455029	-5.621083
C	5.622124	4.455029	5.621083
H	-6.000074	4.395734	-6.453389

H	-6.000074	4.395734	6.453389
H	6.378724	4.460467	-6.408469
H	6.378724	4.460467	6.408469
C	0.850339	5.187219	-4.018859
C	-0.512709	5.196463	-4.013708
C	0.850339	5.187219	4.018859
C	-0.512709	5.196463	4.013708
C	-4.599444	4.937818	-3.370715
C	-4.599444	4.937818	3.370715
C	4.932106	4.965769	-3.342126
C	4.932106	4.965769	3.342126
C	-5.559409	4.933243	-4.391369
C	-5.559409	4.933243	4.391369
C	5.904040	4.981769	-4.351489
C	5.904040	4.981769	4.351489
H	1.510412	5.665262	-4.735782
H	-1.171185	5.684383	-4.725353
H	1.510412	5.665262	4.735782
H	-1.171185	5.684383	4.725353
H	-4.837403	5.418834	-2.422055
H	-4.837403	5.418834	2.422055
H	5.149857	5.447322	-2.388692
H	5.149857	5.447322	2.388692
H	-6.545452	5.362555	-4.201567
H	-6.545452	5.362555	4.201567
H	6.879476	5.428928	-4.149203
H	6.879476	5.428928	4.149203

S7- Ag(111)-TPP

E= -823.67750703 eV Symmetry: C_s

Ag	1.668103	-1.641278	0.000000
Ag	-0.834052	-1.641278	1.444620
Ag	-0.834052	-1.641278	-1.444620
Ag	9.174555	-1.641277	-4.333848
Ag	-8.340500	-1.641277	5.778474
Ag	9.174555	-1.641277	4.333848
Ag	-0.834055	-1.641277	10.112322
Ag	-8.340500	-1.641277	-5.778474
Ag	-0.834055	-1.641277	-10.112322
Ag	11.676708	-1.641274	-5.778467
Ag	-10.842654	-1.641274	7.223092
Ag	11.676708	-1.641274	5.778467
Ag	-0.834054	-1.641274	13.001559
Ag	-10.842654	-1.641274	-7.223092
Ag	-0.834054	-1.641274	-13.001559
Ag	4.170256	-1.641274	-1.444616
Ag	-3.336202	-1.641274	2.889240
Ag	4.170256	-1.641274	1.444616
Ag	-0.834054	-1.641274	4.333856
Ag	-3.336202	-1.641274	-2.889240
Ag	-0.834054	-1.641274	-4.333856
Ag	9.174558	-1.641273	-1.444606
Ag	-5.838345	-1.641273	7.223097
Ag	9.174558	-1.641273	1.444606
Ag	-3.336213	-1.641273	8.667703
Ag	-5.838345	-1.641273	-7.223097
Ag	-3.336213	-1.641273	-8.667703
Ag	6.672402	-1.641271	-2.889230
Ag	-5.838348	-1.641271	4.333854
Ag	6.672402	-1.641271	2.889230
Ag	-0.834054	-1.641271	7.223084
Ag	-5.838348	-1.641271	-4.333854
Ag	-0.834054	-1.641271	-7.223084
Ag	11.676697	-1.641269	-2.889229
Ag	-8.340494	-1.641269	8.667702
Ag	11.676697	-1.641269	2.889229
Ag	-3.336203	-1.641269	11.556930
Ag	-8.340494	-1.641269	-8.667702
Ag	-3.336203	-1.641269	-11.556930
Ag	6.672412	-1.641266	0.000000
Ag	-3.336206	-1.641266	5.778479
Ag	-3.336206	-1.641266	-5.778479
Ag	11.676702	-1.641265	0.000000
Ag	-5.838351	-1.641265	10.112321
Ag	-5.838351	-1.641265	-10.112321
Ag	1.668100	-1.641263	2.889235
Ag	1.668100	-1.641263	-2.889235
Ag	-3.336201	-1.641263	0.000000
Ag	1.668103	-1.641259	5.778477
Ag	4.170256	-1.641259	4.333858
Ag	1.668103	-1.641259	-5.778477
Ag	-5.838359	-1.641259	-1.444619
Ag	4.170256	-1.641259	-4.333858
Ag	-5.838359	-1.641259	1.444619
Ag	1.668099	-1.641254	8.667711
Ag	6.672408	-1.641254	5.778472
Ag	1.668099	-1.641254	-8.667711
Ag	-8.340507	-1.641254	-2.889239
Ag	6.672408	-1.641254	-5.778472
Ag	-8.340507	-1.641254	2.889239
Ag	4.170254	-1.641251	7.223091
Ag	4.170254	-1.641251	-7.223091
Ag	-8.340507	-1.641251	0.000000
Ag	1.668105	-1.641250	11.556939
Ag	9.174550	-1.641250	7.223091
Ag	1.668105	-1.641250	-11.556939
Ag	-10.842655	-1.641250	-4.333848
Ag	9.174550	-1.641250	-7.223091

Ag	-10.842655	-1.641250	4.333848
Ag	4.170250	-1.641246	10.112325
Ag	6.672406	-1.641246	8.667705
Ag	4.170250	-1.641246	-10.112325
Ag	-10.842656	-1.641246	-1.444620
Ag	6.672406	-1.641246	-8.667705
Ag	-10.842656	-1.641246	1.444620
Ag	13.185879	0.422179	-7.543353
Ag	-13.125675	0.422179	7.647630
Ag	13.185879	0.422179	7.543353
Ag	-0.060204	0.422179	15.190983
Ag	-13.125675	0.422179	-7.647630
Ag	-0.060204	0.422179	-15.190983
Ag	7.967890	1.220392	-4.553228
Ag	-7.927156	1.220392	4.623781
Ag	7.967890	1.220392	4.553228
Ag	-0.040734	1.220392	9.177009
Ag	-7.927156	1.220392	-4.623781
Ag	-0.040734	1.220392	-9.177009
Ag	2.652585	1.109313	-1.525809
Ag	-2.647682	1.109313	1.534302
Ag	2.652585	1.109313	1.525809
Ag	-0.004903	1.109313	3.060111
Ag	-2.647682	1.109313	-1.534302
Ag	-0.004903	1.109313	-3.060111
Ag	10.586752	1.278114	-6.048115
Ag	-10.531197	1.278114	6.144339
Ag	10.586752	1.278114	6.048115
Ag	-0.055555	1.278114	12.192454
Ag	-10.531197	1.278114	-6.144339
Ag	-0.055555	1.278114	-12.192454
Ag	5.321744	1.213580	-3.048868
Ag	-5.301269	1.213580	3.084331
Ag	5.321744	1.213580	3.048868
Ag	-0.020475	1.213580	6.133199
Ag	-5.301269	1.213580	-3.084331
Ag	-0.020475	1.213580	-6.133199
Ag	10.633781	1.246795	-3.047499
Ag	-7.956102	1.246795	7.685375
Ag	10.633781	1.246795	3.047499
Ag	-2.677679	1.246795	10.732874
Ag	-7.956102	1.246795	-7.685375
Ag	-2.677679	1.246795	-10.732874
Ag	0.000000	0.986107	0.000000
Ag	5.301928	1.221224	0.000000
Ag	-2.650964	1.221224	4.591604
Ag	-2.650964	1.221224	-4.591604
Ag	13.377237	0.744213	-4.506497
Ag	-10.591360	0.744213	9.331778
Ag	13.377237	0.744213	4.506497
Ag	-2.785877	0.744213	13.838275
Ag	-10.591360	0.744213	-9.331778
Ag	-2.785877	0.744213	-13.838275
Ag	10.604750	1.192095	0.000000
Ag	-5.302375	1.192095	9.183983
Ag	-5.302375	1.192095	-9.183983
Ag	7.970762	1.195784	-1.526104
Ag	-5.307026	1.195784	6.139831
Ag	7.970762	1.195784	1.526104
Ag	-2.663737	1.195784	7.665935
Ag	-5.307026	1.195784	-6.139831
Ag	-2.663737	1.195784	-7.665935
Ag	13.381081	0.722624	-1.505266
Ag	-7.994139	0.722624	10.835723
Ag	13.381081	0.722624	1.505266
Ag	-5.386942	0.722624	12.340989
Ag	-7.994139	0.722624	-10.835723
Ag	-5.386942	0.722624	-12.340989
Ag	2.632687	1.203998	4.559948
Ag	2.632687	1.203998	-4.559948
Ag	-5.265374	1.203998	0.000000
Ag	2.608606	1.238807	7.620201
Ag	5.294985	1.238807	6.069220
Ag	2.608606	1.238807	-7.620201
Ag	-7.903591	1.238807	-1.550982
Ag	5.294985	1.238807	-6.069220
Ag	-7.903591	1.238807	1.550982
Ag	2.586859	1.232308	10.659570
Ag	7.938029	1.232308	7.570071
Ag	2.586859	1.232308	-10.659570
Ag	-10.524888	1.232308	-3.089499
Ag	7.938029	1.232308	-7.570071
Ag	-10.524888	1.232308	3.089499
Ag	5.252888	1.194784	9.098269
Ag	5.252888	1.194784	-9.098269
Ag	-10.505777	1.194784	0.000000
Ag	2.554869	0.199030	13.731559
Ag	10.614444	0.199030	9.078361
Ag	2.554869	0.199030	-13.731559
Ag	-13.169314	0.199030	-4.653198
Ag	10.614444	0.199030	-9.078361
Ag	-13.169314	0.199030	4.653198
Ag	5.182871	0.251160	12.158823
Ag	7.938414	0.251160	10.567909
Ag	5.182871	0.251160	-12.158823
Ag	-13.121285	0.251160	-1.590914
Ag	7.938414	0.251160	-10.567909
Ag	-13.121285	0.251160	1.590914

H	-1.895525	3.735312	5.063171
H	-1.895525	3.735312	-5.063171
H	2.752083	3.732729	5.059262
H	2.752083	3.732729	-5.059262
H	-3.600905	3.922864	6.843675
H	-3.600905	3.922864	-6.843675
H	4.407679	4.013925	6.860815
H	4.407679	4.013925	-6.860815
H	5.530271	3.931102	-1.339215
H	5.530271	3.931102	1.339215
H	-4.672448	3.859610	1.339456
H	-4.672448	3.859610	-1.339456
C	4.675182	4.085752	0.691925
C	4.675182	4.085752	-0.691925
C	-3.826753	4.053162	0.690938
C	-3.826753	4.053162	-0.690938
C	-2.850430	4.216187	4.841017
C	-2.850430	4.216187	-4.841017
C	3.687241	4.252416	4.843167
C	3.687241	4.252416	-4.843167
C	4.624687	4.417369	5.868546
C	4.624687	4.417369	-5.868546
C	-3.810924	4.333997	5.854128
C	-3.810924	4.333997	-5.854128
C	3.330968	4.319916	-1.145430
C	3.330968	4.319916	1.145430
C	-2.489768	4.320487	1.144094
C	-2.489768	4.320487	-1.144094
N	0.419105	4.407650	2.065394
N	0.419105	4.407650	-2.065394
N	2.550977	4.386455	0.000000
N	-1.712154	4.410620	0.000000
H	-0.704076	4.550891	0.000000
C	2.884511	4.585897	2.468871
C	2.884511	4.585897	-2.468871
C	-2.048002	4.582131	2.470076
C	-2.048002	4.582131	-2.470076
H	1.539076	4.502951	0.000000
C	3.911297	4.760995	3.541338
C	3.911297	4.760995	-3.541338
C	-3.080561	4.729295	3.539774
C	-3.080561	4.729295	-3.539774
C	5.835045	5.079115	5.617818
C	5.835045	5.079115	-5.617818
H	6.579345	5.187666	6.409658
H	6.579345	5.187666	-6.409658
C	1.515570	4.783503	2.815636
C	1.515570	4.783503	-2.815636
C	-0.680402	4.778358	2.818113
C	-0.680402	4.778358	-2.818113
C	-5.043488	4.947005	5.593452
C	-5.043488	4.947005	-5.593452
H	-5.804259	5.011337	6.375016
H	-5.804259	5.011337	-6.375016
C	5.115065	5.474178	3.326589
C	5.115065	5.474178	-3.326589
C	6.069658	5.614264	4.341625
C	6.069658	5.614264	-4.341625
C	-4.307252	5.402066	3.318533
C	-4.307252	5.402066	-3.318533
C	-5.280294	5.491789	4.321046
C	-5.280294	5.491789	-4.321046
C	-0.264715	5.458801	4.042624
C	-0.264715	5.458801	-4.042624
C	1.097207	5.465841	4.039218
C	1.097207	5.465841	-4.039218
H	6.991302	6.164591	4.139007
H	6.991302	6.164591	-4.139007
H	5.287407	5.954192	2.362463
H	5.287407	5.954192	-2.362463
H	-0.924017	5.929959	4.765223
H	-0.924017	5.929959	-4.765223
H	1.753796	5.942857	4.760250
H	1.753796	5.942857	-4.760250
H	-4.485105	5.887515	2.358560
H	-4.485105	5.887515	-2.358560
H	-6.220156	6.008118	4.112423
H	-6.220156	6.008118	-4.112423

S8- Benzene Dimer

E= -147.61618987 eV

H	0.965485	-0.839188	2.188888
C	0.436542	-0.932293	1.236708
C	-0.943494	-1.189527	1.222021
H	-1.489074	-1.298908	2.162880
C	-1.623784	-1.302856	-0.000680
H	-2.698982	-1.500725	-0.012122
C	-0.922975	-1.158500	-1.208889
H	-1.452549	-1.243432	-2.161353
C	0.456923	-0.901190	-1.193919
H	1.001834	-0.783792	-2.134307
C	1.136458	-0.787976	0.028824
H	2.209793	-0.580920	0.040502
H	1.553628	4.233294	2.161717
C	1.023484	4.152424	1.209115
C	-0.357054	3.899409	1.193669
H	-0.901908	3.780595	2.133946
C	-1.036919	3.792425	-0.029319

H	-2.110367	3.588855	-0.041031
C	-0.336995	3.938023	-1.237017
H	-0.866234	3.849806	-2.189227
C	1.043533	4.191417	-1.221984
H	1.589460	4.302948	-2.162577
C	1.723888	4.297748	0.001163
H	2.799327	4.492364	0.013014

S9-2H-TPP

E= -521.97873833 eV Symmetry: C_{2v}

C	-2.452318	2.471657	0.019009
C	-2.907704	1.136394	0.006986
C	-1.093497	2.874835	0.036864
C	-4.270732	0.688210	-0.093962
C	-4.270732	-0.688210	-0.093962
C	-2.907704	-1.136394	0.006986
C	-0.680818	4.275988	0.147679
C	0.680818	4.275988	0.147679
C	1.093497	2.874835	0.036864
N	-2.123466	0.000000	0.064439
H	-1.104977	0.000000	0.075067
H	-5.128234	1.348272	-0.176076
H	-5.128234	-1.348272	-0.176076
N	0.000000	2.040719	-0.017192
H	-1.346545	5.129081	0.239989
H	1.346545	5.129081	0.239989
C	-2.452318	-2.471657	0.019009
C	-1.093497	-2.874835	0.036864
C	-0.680818	-4.275988	0.147679
C	0.680818	-4.275988	0.147679
C	1.093497	-2.874835	0.036864
N	0.000000	-2.040719	-0.017192
H	-1.346545	-5.129081	0.239989
H	1.346545	-5.129081	0.239989
C	2.452318	2.471657	0.019009
C	4.270732	0.688210	-0.093962
C	4.270732	-0.688210	-0.093962
C	2.907704	-1.136394	0.006986
N	2.123466	0.000000	0.064439
H	5.128234	-1.348272	-0.176076
C	2.452318	-2.471657	0.019009
C	2.907704	1.136394	0.006986
H	5.128234	1.348272	-0.176076
H	1.104977	0.000000	0.075067
C	3.508973	3.535430	0.009818
C	3.608055	4.440097	-1.065809
C	4.425488	3.650022	1.073830
C	4.597645	5.432205	-1.078128
C	5.413301	4.644195	1.065277
C	5.503858	5.538833	-0.011872
H	2.897836	4.358176	-1.890858
H	4.353843	2.951491	1.910021
H	4.662405	6.120333	-1.923896
H	6.108287	4.723348	1.904178
H	6.274368	6.313572	-0.019994
C	3.508973	-3.535430	0.009818
C	3.608055	-4.440097	-1.065809
C	4.425488	-3.650022	1.073830
C	4.597645	-5.432205	-1.078128
C	5.413301	-4.644195	1.065277
C	5.503858	-5.538833	-0.011872
H	2.897836	-4.358176	-1.890858
H	4.353843	-2.951491	1.910021
H	4.662405	-6.120333	-1.923896
H	6.108287	-4.723348	1.904178
H	6.274368	-6.313572	-0.019994
C	-3.508973	3.535430	0.009818
C	-3.608055	4.440097	-1.065809
C	-4.425488	3.650022	1.073830
C	-4.597645	5.432205	-1.078128
C	-5.413301	4.644195	1.065277
C	-5.503858	5.538833	-0.011872
H	-2.897836	4.358176	-1.890858
H	-4.353843	2.951491	1.910021
H	-4.662405	6.120333	-1.923896
H	-6.108287	4.723348	1.904178
H	-6.274368	6.313572	-0.019994
C	-3.508973	-3.535430	0.009818
C	-3.608055	-4.440097	-1.065809
C	-4.425488	-3.650022	1.073830
C	-4.597645	-5.432205	-1.078128
C	-5.413301	-4.644195	1.065277
C	-5.503858	-5.538833	-0.011872
H	-2.897836	-4.358176	-1.890858
H	-4.353843	-2.951491	1.910021
H	-4.662405	-6.120333	-1.923896
H	-6.108287	-4.723348	1.904178
H	-6.274368	-6.313572	-0.019994

S10- Cu(111)-166 Surface Cluster

E= -429.86498153 eV Symmetry: C_s

Cu	8.105765	-1.142575	6.381640
Cu	8.105765	-1.142575	-6.381640
Cu	1.473780	-1.142575	10.210618
Cu	1.473780	-1.142575	-10.210618
Cu	-9.579545	-1.142575	-3.828978
Cu	-9.579545	-1.142575	3.828978
Cu	5.895106	-1.142573	7.657964

Cu	5.895106	-1.142573	-7.657964
Cu	3.684439	-1.142573	8.934294
Cu	3.684439	-1.142573	-8.934294
Cu	-9.579545	-1.142573	-1.276329
Cu	-9.579545	-1.142573	1.276329
Cu	5.895105	-1.142571	5.105304
Cu	5.895105	-1.142571	-5.105304
Cu	1.473770	-1.142571	7.657963
Cu	1.473770	-1.142571	-7.657963
Cu	-7.368876	-1.142571	-2.552659
Cu	-7.368876	-1.142571	2.552659
Cu	10.316433	-1.142569	-5.105310
Cu	10.316433	-1.142569	5.105310
Cu	3.684438	-1.142569	6.381633
Cu	3.684438	-1.142569	-6.381633
Cu	-0.736888	-1.142569	11.486948
Cu	-0.736888	-1.142569	-11.486948
Cu	-7.368876	-1.142569	0.000000
Cu	-9.579545	-1.142569	6.381637
Cu	-9.579545	-1.142569	-6.381637
Cu	3.684442	-1.142567	3.828982
Cu	3.684442	-1.142567	-3.828982
Cu	1.473774	-1.142567	5.105311
Cu	1.473774	-1.142567	-5.105311
Cu	-5.158216	-1.142567	-1.276329
Cu	-5.158216	-1.142567	1.276329
Cu	8.105764	-1.142566	-3.828979
Cu	8.105764	-1.142566	3.828979
Cu	-0.736889	-1.142566	8.934287
Cu	-0.736889	-1.142566	-8.934287
Cu	-7.368876	-1.142566	5.105308
Cu	-7.368876	-1.142566	-5.105308
Cu	10.316432	-1.142565	-2.552650
Cu	10.316432	-1.142565	2.552650
Cu	-2.947556	-1.142565	10.210617
Cu	-2.947556	-1.142565	-10.210617
Cu	-7.368876	-1.142565	7.657967
Cu	-7.368876	-1.142565	-7.657967
Cu	5.895101	-1.142564	2.552657
Cu	5.895101	-1.142564	-2.552657
Cu	-0.736884	-1.142564	6.381636
Cu	-0.736884	-1.142564	-6.381636
Cu	-5.158216	-1.142564	3.828978
Cu	-5.158216	-1.142564	-3.828978
Cu	8.105768	-1.142563	1.276328
Cu	8.105768	-1.142563	-1.276328
Cu	1.473774	-1.142563	2.552651
Cu	1.473774	-1.142563	-2.552651
Cu	-2.947547	-1.142563	0.000000
Cu	-2.947552	-1.142563	7.657965
Cu	-2.947552	-1.142563	-7.657965
Cu	-5.158216	-1.142563	6.381637
Cu	-5.158216	-1.142563	-6.381637
Cu	3.684441	-1.142562	1.276321
Cu	3.684441	-1.142562	-1.276321
Cu	-0.736894	-1.142562	3.828980
Cu	-0.736894	-1.142562	-3.828980
Cu	-2.947547	-1.142562	2.552659
Cu	-2.947547	-1.142562	-2.552659
Cu	10.316427	-1.142561	0.000000
Cu	-5.158214	-1.142561	8.934288
Cu	-5.158214	-1.142561	-8.934288
Cu	5.895100	-1.142560	0.000000
Cu	1.473778	-1.142560	0.000000
Cu	-0.736889	-1.142560	1.276329
Cu	-0.736889	-1.142560	-1.276329
Cu	-2.947550	-1.142560	5.105306
Cu	-2.947550	-1.142560	-5.105306
Cu	8.842651	0.941652	7.657964
Cu	8.842651	0.941652	-7.657964
Cu	2.210666	0.941652	11.486943
Cu	2.210666	0.941652	-11.486943
Cu	-11.053317	0.941652	-3.828978
Cu	-11.053317	0.941652	3.828978
Cu	6.631992	0.941654	8.934289
Cu	6.631992	0.941654	-8.934289
Cu	4.421325	0.941654	10.210618
Cu	4.421325	0.941654	-10.210618
Cu	-11.053317	0.941654	-1.276329
Cu	-11.053317	0.941654	1.276329
Cu	6.631996	0.941656	6.381637
Cu	6.631996	0.941656	-6.381637
Cu	2.210661	0.941656	8.934296
Cu	2.210661	0.941656	-8.934296
Cu	-8.842658	0.941656	-2.552659
Cu	-8.842658	0.941656	2.552659
Cu	11.053319	0.941658	-6.381635
Cu	11.053319	0.941658	6.381635
Cu	4.421329	0.941658	7.657966
Cu	4.421329	0.941658	-7.657966
Cu	-0.000002	0.941658	12.763272
Cu	-0.000002	0.941658	-12.763272
Cu	-8.842658	0.941658	0.000000
Cu	-11.053317	0.941658	6.381637
Cu	-11.053317	0.941658	-6.381637
Cu	4.421328	0.941660	5.105306
Cu	4.421328	0.941660	-5.105306
Cu	2.210661	0.941660	6.381635

Cu	2.210661	0.941660	-6.381635
Cu	-6.631989	0.941660	-1.276329
Cu	-6.631989	0.941660	1.276329
Cu	8.842655	0.941661	-5.105312
Cu	8.842655	0.941661	5.105312
Cu	0.000003	0.941661	10.210620
Cu	0.000003	0.941661	-10.210620
Cu	-8.842658	0.941661	5.105308
Cu	-8.842658	0.941661	-5.105308
Cu	11.053323	0.941662	-3.828983
Cu	11.053323	0.941662	3.828983
Cu	-2.210665	0.941662	11.486950
Cu	-2.210665	0.941662	-11.486950
Cu	-8.842658	0.941662	7.657967
Cu	-8.842658	0.941662	-7.657967
Cu	6.631987	0.941663	-3.828981
Cu	6.631987	0.941663	3.828981
Cu	0.000002	0.941663	7.657960
Cu	0.000002	0.941663	-7.657960
Cu	-6.631989	0.941663	3.828978
Cu	-6.631989	0.941663	-3.828978
Cu	2.210665	0.941664	3.828984
Cu	2.210665	0.941664	-3.828984
Cu	-4.421330	0.941664	0.000000
Cu	8.842655	0.941665	-2.552652
Cu	8.842655	0.941665	2.552652
Cu	4.421332	0.941665	2.552654
Cu	4.421332	0.941665	-2.552654
Cu	-0.000003	0.941665	5.105313
Cu	-0.000003	0.941665	-5.105313
Cu	-2.210666	0.941665	8.934289
Cu	-2.210666	0.941665	-8.934289
Cu	-4.421330	0.941665	2.552659
Cu	-4.421330	0.941665	-2.552659
Cu	-6.631989	0.941665	6.381637
Cu	-6.631989	0.941665	-6.381637
Cu	11.053313	0.941666	-1.276327
Cu	11.053313	0.941666	1.276327
Cu	-4.421325	0.941666	10.210614
Cu	-4.421325	0.941666	-10.210614
Cu	-6.631989	0.941666	8.934286
Cu	-6.631989	0.941666	-8.934286
Cu	6.631991	0.941667	1.276330
Cu	6.631991	0.941667	-1.276330
Cu	-2.210662	0.941667	6.381638
Cu	-2.210662	0.941667	-6.381638
Cu	-4.421330	0.941667	5.105308
Cu	-4.421330	0.941667	-5.105308
Cu	8.842659	0.941668	0.000000
Cu	2.210664	0.941668	1.276323
Cu	2.210664	0.941668	-1.276323
Cu	-0.000004	0.941668	2.552653
Cu	-0.000004	0.941668	-2.552653
Cu	-2.210660	0.941668	1.276329
Cu	-2.210660	0.941668	-1.276329
Cu	-4.421329	0.941668	7.657967
Cu	-4.421329	0.941668	-7.657967
Cu	4.421323	0.941669	0.000000
Cu	-2.210661	0.941669	3.828978
Cu	-2.210661	0.941669	-3.828978
Cu	0.000000	0.941670	0.000000

S11- Ag(111)-166 Surface Cluster

E= -298.19021653 eV Symmetry: C_s

Ag	1.668103	-1.641278	0.000000
Ag	-0.834052	-1.641278	1.444620
Ag	-0.834052	-1.641278	-1.444620
Ag	9.174555	-1.641277	-4.333848
Ag	-8.340500	-1.641277	5.778474
Ag	9.174555	-1.641277	4.333848
Ag	-0.834055	-1.641277	10.112322
Ag	-8.340500	-1.641277	-5.778474
Ag	-0.834055	-1.641277	-10.112322
Ag	11.676708	-1.641274	-5.778467
Ag	-10.842654	-1.641274	7.223092
Ag	11.676708	-1.641274	5.778467
Ag	-0.834054	-1.641274	13.001559
Ag	-10.842654	-1.641274	-7.223092
Ag	-0.834054	-1.641274	-13.001559
Ag	4.170256	-1.641274	-1.444616
Ag	-3.336202	-1.641274	2.889240
Ag	4.170256	-1.641274	1.444616
Ag	-0.834054	-1.641274	4.333856
Ag	-3.336202	-1.641274	-2.889240
Ag	-0.834054	-1.641274	-4.333856
Ag	9.174558	-1.641273	-1.444606
Ag	-5.838345	-1.641273	7.223097
Ag	9.174558	-1.641273	1.444606
Ag	-3.336213	-1.641273	8.667703
Ag	-5.838345	-1.641273	-7.223097
Ag	-3.336213	-1.641273	-8.667703
Ag	6.672402	-1.641271	-2.889230
Ag	-5.838348	-1.641271	4.333854
Ag	6.672402	-1.641271	2.889230
Ag	-0.834054	-1.641271	7.223084
Ag	-5.838348	-1.641271	-4.333854
Ag	-0.834054	-1.641271	-7.223084
Ag	11.676697	-1.641269	-2.889229

Ag	-8.340494	-1.641269	8.667702
Ag	11.676697	-1.641269	2.889229
Ag	-3.336203	-1.641269	11.556930
Ag	-8.340494	-1.641269	-8.667702
Ag	-3.336203	-1.641269	-11.556930
Ag	6.672412	-1.641266	0.000000
Ag	-3.336206	-1.641266	5.778479
Ag	-3.336206	-1.641266	-5.778479
Ag	11.676702	-1.641265	0.000000
Ag	-5.838351	-1.641265	10.112321
Ag	-5.838351	-1.641265	-10.112321
Ag	1.668100	-1.641263	2.889235
Ag	1.668100	-1.641263	-2.889235
Ag	-3.336201	-1.641263	0.000000
Ag	1.668103	-1.641259	5.778477
Ag	4.170256	-1.641259	4.333858
Ag	1.668103	-1.641259	-5.778477
Ag	-5.838359	-1.641259	-1.444619
Ag	4.170256	-1.641259	-4.333858
Ag	-5.838359	-1.641259	1.444619
Ag	1.668099	-1.641254	8.667711
Ag	6.672408	-1.641254	5.778472
Ag	1.668099	-1.641254	-8.667711
Ag	-8.340507	-1.641254	-2.889239
Ag	6.672408	-1.641254	-5.778472
Ag	-8.340507	-1.641254	2.889239
Ag	4.170254	-1.641251	7.223091
Ag	4.170254	-1.641251	-7.223091
Ag	-8.340507	-1.641251	0.000000
Ag	1.668105	-1.641250	11.556939
Ag	9.174550	-1.641250	7.223091
Ag	1.668105	-1.641250	-11.556939
Ag	-10.842655	-1.641250	-4.333848
Ag	9.174550	-1.641250	-7.223091
Ag	-10.842655	-1.641250	4.333848
Ag	4.170250	-1.641246	10.112325
Ag	6.672406	-1.641246	8.667705
Ag	4.170250	-1.641246	-10.112325
Ag	-10.842656	-1.641246	-1.444620
Ag	6.672406	-1.641246	-8.667705
Ag	-10.842656	-1.641246	1.444620
Ag	13.185879	0.422179	-7.543353
Ag	-13.125675	0.422179	7.647630
Ag	13.185879	0.422179	7.543353
Ag	-0.060204	0.422179	15.190983
Ag	-13.125675	0.422179	-7.647630
Ag	-0.060204	0.422179	-15.190983
Ag	7.967890	1.220392	-4.553228
Ag	-7.927156	1.220392	4.623781
Ag	7.967890	1.220392	4.553228
Ag	-0.040734	1.220392	9.177009
Ag	-7.927156	1.220392	-4.623781
Ag	-0.040734	1.220392	-9.177009
Ag	2.652585	1.109313	-1.525809
Ag	-2.647682	1.109313	1.534302
Ag	2.652585	1.109313	1.525809
Ag	-0.004903	1.109313	3.060111
Ag	-2.647682	1.109313	-1.534302
Ag	-0.004903	1.109313	-3.060111
Ag	10.586752	1.278114	-6.048115
Ag	-10.531197	1.278114	6.144339
Ag	10.586752	1.278114	6.048115
Ag	-0.055555	1.278114	12.192454
Ag	-10.531197	1.278114	-6.144339
Ag	-0.055555	1.278114	-12.192454
Ag	5.321744	1.213580	-3.048868
Ag	-5.301269	1.213580	3.084331
Ag	5.321744	1.213580	3.048868
Ag	-0.020475	1.213580	6.133199
Ag	-5.301269	1.213580	-3.084331
Ag	-0.020475	1.213580	-6.133199
Ag	10.633781	1.246795	-3.047499
Ag	-7.956102	1.246795	7.685375
Ag	10.633781	1.246795	3.047499
Ag	-2.677679	1.246795	10.732874
Ag	-7.956102	1.246795	-7.685375
Ag	-2.677679	1.246795	-10.732874
Ag	0.000000	0.986107	0.000000
Ag	5.301928	1.221224	0.000000
Ag	-2.650964	1.221224	4.591604
Ag	-2.650964	1.221224	-4.591604
Ag	13.377237	0.744213	-4.506497
Ag	-10.591360	0.744213	9.331778
Ag	13.377237	0.744213	4.506497
Ag	-2.785877	0.744213	13.838275
Ag	-10.591360	0.744213	-9.331778
Ag	-2.785877	0.744213	-13.838275
Ag	10.604750	1.192095	0.000000
Ag	-5.302375	1.192095	9.183983
Ag	-5.302375	1.192095	-9.183983
Ag	7.970762	1.195784	-1.526104
Ag	-5.307026	1.195784	6.139831
Ag	7.970762	1.195784	1.526104
Ag	-2.663737	1.195784	7.665935
Ag	-5.307026	1.195784	-6.139831
Ag	-2.663737	1.195784	-7.665935
Ag	13.381081	0.722624	-1.505266
Ag	-7.994139	0.722624	10.835723

Ag	13.381081	0.722624	1.505266
Ag	-5.386942	0.722624	12.340989
Ag	-7.994139	0.722624	-10.835723
Ag	-5.386942	0.722624	-12.340989
Ag	2.632687	1.203998	4.559948
Ag	2.632687	1.203998	-4.559948
Ag	-5.265374	1.203998	0.000000
Ag	2.608606	1.238807	7.620201
Ag	5.294985	1.238807	6.069220
Ag	2.608606	1.238807	-7.620201
Ag	-7.903591	1.238807	-1.550982
Ag	5.294985	1.238807	-6.069220
Ag	-7.903591	1.238807	1.550982
Ag	2.586859	1.232308	10.659570
Ag	7.938029	1.232308	7.570071
Ag	2.586859	1.232308	-10.659570
Ag	-10.524888	1.232308	-3.089499
Ag	7.938029	1.232308	-7.570071
Ag	-10.524888	1.232308	3.089499
Ag	5.252888	1.194784	9.098269
Ag	5.252888	1.194784	-9.098269
Ag	-10.505777	1.194784	0.000000
Ag	2.554869	0.199030	13.731559
Ag	10.614444	0.199030	9.078361
Ag	2.554869	0.199030	-13.731559
Ag	-13.169314	0.199030	-4.653198
Ag	10.614444	0.199030	-9.078361
Ag	-13.169314	0.199030	4.653198
Ag	5.182871	0.251160	12.158823
Ag	7.938414	0.251160	10.567909
Ag	5.182871	0.251160	-12.158823
Ag	-13.121285	0.251160	-1.590914
Ag	7.938414	0.251160	-10.567909
Ag	-13.121285	0.251160	1.59091

References

[1] te Velde, G.; Bickelhaupt, F. M.; Baerends, E. J.; Fonseca Guerra, C.; van Gisbergen, S. J. A.; Snijders, J. G.; Ziegler, T. Chemistry with ADF. *J. Comput. Chem.* **22,** 931–967 (2001).

[2] Baerends, E. J.; Autschbach, J.; Bérces, A.; Bickelhaupt, F. M.; Bo, C.; Boerrigter, P. M.; Cavallo, L.; Chong, D. P.; Deng, L.; Dickson, R. M.; et al. ADF2010.01, SCM, Theoretical Chemistry, Vrije Universiteit, Amsterdam, The Netherlands, http://www.scm.com.

[3] Perdew, J. P.; Burke, K.; Wang, Y. Generalized Gradient Approximation for the Exchange-Correlation Hole of a Many-Electron System. *Phys. Rev. B* **54,** 16533–16539 (1996).

[4] Zhang, Y.; Yang, W. Comment on Generalized Gradient Approximation Made Simple. *Phys. Rev. Lett.* **80,** 89 (1998).

[5] Perdew, J. P.; Burke, K.; Ernzerhof, M. Reply to Comment on Generalized Gradient Approximation Made Simple. *Phys. Rev. Lett.* **80,** 891 (1998).

[6] Hammer, B.; Hansen, L. B.; Norskov, J. K. Improved Adsorption Energetics within Density-Functional Theory using Revised Perdew-Burke-Ernzerhof Functionals. *Phys. Rev. B* **59,** 7413–7421. (1999).

[7] Grimme, S.; Antony, J., Ehrlich, S.; Krieg, H. A consistent and accurate ab initio parameterization of density functional dispersion correction (DFT-D) for the 94 elements H-Pu. *J. Chem. Phys.* **132,** 154104 (2010).

[8] Suh, I.; Ohta, H.; Waseda, Y. High-temperature thermal expansion of six metallic elements measured by dilatation method and X-ray diffraction. *J. Mater. Sci.* **23,** 757-760 (1988).

[9] Pitoňák, M.; Neogrády, P.; Řezáč, J.; Jurečka, P.; Urban, M.; Hobza, P. Benzene Dimer: High-Level Wave Funtion and Density Functional Theory Calculations. **4,** 1829-1834 (2008).

[10] Lomas, J. R.; Baddeley, C. J.; Tikhov, M. S.; Lambert, R M. Ethyne Cyclization to Benzene over Cu(110). *Langmuir.* **11,** 3048-3053 (1995).

[11] (a) Lukas, S.; Witte, G.; Wöll, C. Adsorption of acenes on flat and vicinal Cu(111) surfaces: Step induced formation of lateral order. J. Chem. Phys. **114,** 10123 (2001).
(b) Xi, M.; Yang, M. X.; Jo, S. K.; Bent, B. E.; Stevens, P. Benzene adsorption on Cu(111):Formation of a stable bilayer. *J. Chem. Phys.* **101,** 9122 (1994)

[12] Witte, G.; Lukas, S.; Bagus, P. S.; Wöll, C. Vacuum level alignment at organic/metal junctions: "Cushion" effect and the interface dipole. *Appl. Phys. Lett*. **87**, 263502 (2005)

[13] Triguero, L.; Föhlisch, A.; Vaterlaein, P.; Hasselström, J.; Weinelt, M.; Petterson, L. G. M.; Luo, Y.; Agren, H.; Nilsson, A. Direct Measurement of Donation/Back-Donation in Unsaturated Hydrocarbon Bonding to Metals. *J. Am. Chem. Soc*. **122**, 12310-12316 (2000).

[14] Bickelhaupt, F. M.; Baerends, E. J. Kohn-Sham Density Functional Theory: Predicting and Understanding Chemistry. *Rev. Comp. Chem.* **15,** 1-86 (2000).

[15] Hoffmann, R. A chemical and theoretical way to look at bonding on surfaces. *Rev. Mod. Phys.* **60**, 601-628 (1988).

[16] Glassey, W. G.; Hoffmann, R. A Cinoaratuve Study of p(2x2)-CO/M(111), M=Pt,Cu,Al Chemisorption Systems. *J. Phys. Chem. B* **105**, 3245-3260 (2001).

[17] Philipsen, P. H. T.; Baerends, E. J. The role of the Fermi surface in adsorbate-metal interaction: an energy decomposition analysis. *J. Phys. Chem. B* **110***,* 12470-12479 (2006).

[18] Glassey, W. G. Energy Partitioning Studies of CO and NO Chemisorption on the Pd(111) Surface. *J. Phy. Chem. B* **108,** 5967-5979 (2004).

[19] Wiberg, K. B.; Rablen, P. R. Comparison of Atomic Charges Derived via Different Procedures*. J. Comput. Chem*. **14**, 1504-1518 (1993).